2014-12-01

Investigating the Relationship Between High Temperature Flow Stress and Friction Stir Weldability in HSLA Steels

David Jordan Walser
Brigham Young University

Investigating the Relationship Between High Temperature Flow Stress and Friction Stir Weldability in HSLA Steels

D. Jordan Walser

A thesis submitted to the faculty of
Brigham Young University
in partial fulfillment of the requirements for the degree of

Master of Science

Carl D. Sorensen, Chair
Tracy W. Nelson
David T. Fullwood

Department of Mechanical Engineering

Brigham Young University

December 2014

ABSTRACT

Investigating the Relationship Between High Temperature Flow Stress
and Friction Stir Weldability in HSLA Steels

D. Jordan Walser
Department of Mechanical Engineering, BYU
Master of Science

The feed rate at which a defect free friction stir weld can be run (friction stir weldability) on an HSLA steel plate can vary widely between heats that meet the same specified physical properties. Consequently, every time a new heat of HSLA steel is obtained, exploratory welds must be run to determine the proper feed rate for that plate. Previous research suggests that the varying levels of alloying elements related to high temperature physical properties between the different heats causes the observed change in friction stir weldability. Because of this, it was hypothesized that the high temperature physical properties of HSLA steels are related to their friction stir weldability.

High temperature physical propeties of HSLA steels are a function of the alloying content of the steel. To determine the relationship between high temperature physical properties and alloying content, eight different heats of HSLA steel with different chemical compositions were obtained. In particular, percent additions of molybdenum, vanadium, niobium, and titanium were varied between the heats in a factorial design. Gleeble compression tests were run on each heat to determine their high temperature properties. Based on these tests, experimental models were constructed to estimate the high temperature properties of HSLA steels based on composition and temperature. These models were used to determine the high temperature physical properties of HSLA heats with known friction stir weldability. The high temperature physical properties were compared to the friction stir weldability of each heat. No correlation was found in this study between the high temperature properties examined and friction stir weldability in HSLA steels.

Keywords: FSW, HSLA, alloying elements, gleeble, high temperature physical properties, linear model

ACKNOWLEDGMENTS

I would like to thank my committee for their advice and direction on my research and in writing this thesis. I would also like to thank my wife, whose support and advice helped me greatly in getting my Master's thesis completed.

Funding and materials for this work were provided by the Center for Friction Stir Processing, an NSF I/UCRC. My work would not have been possible without them, and I thank them for that support.

TABLE OF CONTENTS

LIST OF TABLES

LIST OF FIGURES

CHAPTER 1. INTRODUCTION

High-strength low-alloy (HSLA) steels are a class of steels characterized by having high strength and toughness due to their low carbon content and carefully refined microstructure. HSLA steels are used in applications that require a high weight to strength ratio or that need to handle high stress, such as cars, trucks, bridges, and oil pipelines.

Traditional fusion joining methods, such as arc welding, degrade the refined microstructure of HSLA steels. This leads to decreased material performance in the weld when compared to the base metal. To avoid the negative effects of fusion welding on HSLA steels, Friction Stir Welding (FSW), a solid state process, has been proposed as an alternative joining method.

It has been noted that different heats of HSLA steels that meet the same specifications for physical properties (yield strength, hardness, etc.) often vary in the rate at which quality friction stir welds can be produced (friction stir weldability). It is suspected that this wide variability in friction stir weldability is linked to the broad chemical composition specifications for HSLA steels. Under current HSLA classifications, alloying content can vary widely between heats of the same classification [1], causing uncertainty in the optimum running speed of the weld. Previous research done at BYU, using five different alloys of HSLA steels, has shown a correlation between molybdenum and vanadium content and friction stir weldability. No other correlations tried, including A1 or A3 temperatures, or carbon equivalent (CE) fit the data [2]. It has been hypothesized that the high temperature strengthening effect of molybdenum and vanadium is the driver for the change in friction stir weldability of those HSLA heats.

1.1 About this Thesis

This study explores the relationship in HSLA steels between chemical composition and high temperature properties to determine if high temperature properties drive friction stir weldability. Eight heats of carefully varied chemical composition were created for testing. The heats'

high temperature properties were tested using a Gleeble 3500 system to heat and then compress samples made from each steel type. Based on the results of the compression tests, linear models were created that accurately predict high temperature physical properties in HSLA steels as a function of alloying composition and testing temperature. These models were used to estimate the high temperature physical properties of five alloys with known friction stir weldability. By performing statistical analysis, we explored the relationship between the alloys' known friction stir weldability and predicted high temperature physical properties. Based on this research, we have not found a statistically significant correlation between high temperature properties and friction stir weldability in HSLA steels.

As a secondary result of this study, we have developed experimental models for the estimation of high temperature yield stress, maximum stress, and hardening rate constant (the properties examined) of HSLA steels based on composition and temperature.

1.1.1 Organization of Thesis

This thesis is organized into chapters. Chapter 1 introduces the study area and study focus for this thesis. Chapter 2 gives the necessary background for understanding the study area, including information on HSLA steels, their joining methods, and preliminary research in this area. The methods used in this study, to determine both friction stir weldability and high temperature properties, are detailed in Chapter 3. The results of the study and a discussion of the results, including detailing our experimental model to estimate several high temperature properties of HSLA steels, are in Chapter 4. Concluding remarks are contained in Chapter 5.

CHAPTER 2. BACKGROUND

This thesis seeks to explore the relationship between the high temperature physical properties of HSLA steels and their friction stir weldability, or the maximum travel speed at which quality friction stir welds (defined as those without a visible lack-of-consolidation defect) can be created. Pursuant to this goal, this chapter contains relevant information on HSLA steels in the context of this research. Included is a section on the effects of the alloying elements focused on in this study, a section on traditional fusion joining methods for HSLA steels, a section on friction stir welding and HSLA steels, and a review of previous research in this topic area.

2.1 High-Strength Low-Alloy Steels

HSLA steels are characterized by high strength, toughness, and formability. These properties come from a low carbon content and the addition of micro-alloying elements to form carbides that precipitate strengthen and refine the grain size of the microstructure [3]. The carbon content in HSLA steel ranges from 0.03 to 0.3 percent, and the common micro-alloying elements include molybdenum, vanadium, niobium, and titanium.

2.1.1 Micro-Alloying Elements

Molybdenum, vanadium, and niobium can increase the elevated temperature properties of the steel, such as tensile strength [4]. The motivation for this study was to determine if this increased strength at the high temperatures at which welds are run is the driving mechanism for the change in friction stir weldability of HSLA steels at different compositions.

Molybdenum increases the hot temperature strength and creep resistance of steels. Molybdenum in the 0.15-0.3 percent range increases the solubility of niobium and vanadium in austenite, allowing more to precipitate. This is thought to be one of the main factors in molybdenum's strengthening of HSLA steels [5].

Vanadium increases strength without impairing notch toughness in steels. It does this through grain refinement and precipitation hardening. Vanadium is used in some HSLA steels in concentrations up to 0.12 percent [6], and is also added to improve high temperature strength [4].

Niobium increases strength through grain refinement and precipitation strengthening. It is a more efficient grain refiner than vanadium [5]. It is also added to improve the high temperature strength of the steel [4].

Titanium retards the growth of grains in austenite. It also forms precipitates that help grain refine and strengthen the steel. It improves the performance of niobium by bonding with nitrogen, allowing niobium to form more Nb(CN) particles in the ferrite [5].

2.1.2 Thermomechanically Controlled Processing

The refined microstructure necessary for strength and toughness of HSLA steels is developed by thermomechanically controlled processing (TMCP) [5,7]. This microstructure is obtained through repeated rolling near the A3 temperature, followed by accelerated cooling [3]. During the austenite phase of the controlled rolling, the microalloying elements form fine precipitates in the austenitic matrix. These precipitates migrate to energetically favorable spots, normally along the grain boundaries. These precipitates limit grain growth by pinning the austenite grain boundaries [8].

Because the desirable properties of HSLA steels are based primarily on microstructures developed during TMCP, the chemical composition specifications are more lax for HSLA steels than other classifications [5]. The same grain size can be obtained with various levels of the grain refining elements. Because of this, the chemical composition can vary even between heats of the same steel from a manufacturer.

2.2 Fusion Welding

Post processes, like fusion welding, which disrupt the refined microstructure of the HSLA steel, are detrimental to the strength and toughness of the material [1]. In fusion welding, heat sufficient to melt the materials to be joined is applied along the joining area. This results in three zones of differing microstructure: a fusion zone, a heat affected zone (HAZ), and the base metal.

In the fusion zone, the metal melts and is mixed with a filler metal, changing the chemical composition of the weld, resulting in a coarse grain cast microstructure. The filler acts as an alloying agent, and can mitigate some of the loss of strength and toughness that comes from the coarsening of the microstructure [8].

Because of the high heat input in the HAZ from the molten metal of the fusion zone, the precipitates at the grain boundaries coarsen and dissolve, lessening their ability to pin the austenite grain boundaries. This allows the austenite grains to grow, resulting in a coarser grained microstructure [8]. The high heat input of fusion welds can lead to the formation of bainite and martensite in the HAZ, which reduce the ductility and increase the hardness of the metal [8, 9]. Careful control of heat input and cooling rate are needed in fusion welding to minimize the adverse effects on the microstructure by reducing the HAZ width and to avoid the adverse phase changes in the HAZ [10, 11].

2.3 Friction Stir Welding

Friction stir welding is a relatively new solid-state welding method developed by The Welding Institute in 1991 [12]. Joining is accomplished by a rotating tool, which, when plunged into the materials to be joined, generates localized heat through friction. The heat softens the material and allows the tool to stir the materials together. Because this is a solid-state process, the problems of the fusion zone associated with a cast microstructure are avoided. The stir zone can exhibit a more refined microstructure than the base metal. The peak temperature of the process is lower than the melting temperature of the material [13, 14], lessening the property degradation in the HAZ [15] when compared to fusion welding. Most research in FSW has been done with lighter alloys, such as aluminum, but research in steels has shown promise. The joining tool must be made of a material with a higher melting temperature than the material to be joined. In steels, the tool is made of a material with high temperature resistance, like polycrystalline cubic boron nitride (PCBN) [16].

2.4 Friction Stir Weldability of HSLA Steels

A preliminary study on the friction stir weldability of HSLA steels was conducted at Brigham Young University in 2010 [2]. The chemical compositions of the five alloys used in

the study can be found in Table 2.1. The friction stir weldability of each alloy was determined by running bead on plate welds at increasing travel speeds and varying spindle speeds until defects began to occur in the weld. The highest travel speed at which a quality weld could be performed was recorded as the weldability of that alloy. The parameter combinations used for three of the preliminary alloys can be seen in Figure 2.1 on page 7.

Table 2.1: Chemical composition of the 5 HSLA alloys used in the preliminary study. Highlighted are the 4 elements focused on in this study.

Element/Alloy	**X-65**	**HSLA-65**	**X-80**	**L-80**	**NGS Alloy**
C	0.054	0.077	0.04	0.266	0.21
Mn	1.26	1.39	1.7	1.34	1.28
Si	0.286	0.248	0.135	0.238	0.23
Ni	0.163	0.33	0.147	0.012	0.13
Cr	0.028	0.147	0.41	0.188	0.14
Cu	0.303	0.253	0.263	0.015	0.22
Al	0.028	0.016	0.031	0.028	0.035
Mo	0.005	0.064	0.005	0.04	0.04
V	0.03	0.058	0.002	0.003	0.02
Nb	0.05	0.02	0.102	0.002	0.001
Ti	0.013	0.012	0.014	0.003	0.003
N	0.07	0.011	0.006	0.009	
P	0.005	0.011	0.013	0.008	0.013
S	0.005	0.006	0.001	0.006	0.001

Different correlations were attempted to relate differences between the heats to the observed friction stir weldability of each alloy. The A3 temperatures and the Carbon Equivalent (CE) of the heats did not correlate with the friction stir weldability data. When chemical composition was examined, it was discovered that there was a correlation between friction stir weldability and total molybdenum and vanadium content. This correlation can be seen in Figure 2.2 on page 8. Molybdenum and vanadium are known to increase high temperature strength of HSLA steels. Based on this observed correlation, it was decided to focus this study on examining the relationship between high temperature strengthening alloying agents and the friction stir weldability of HSLA steels.

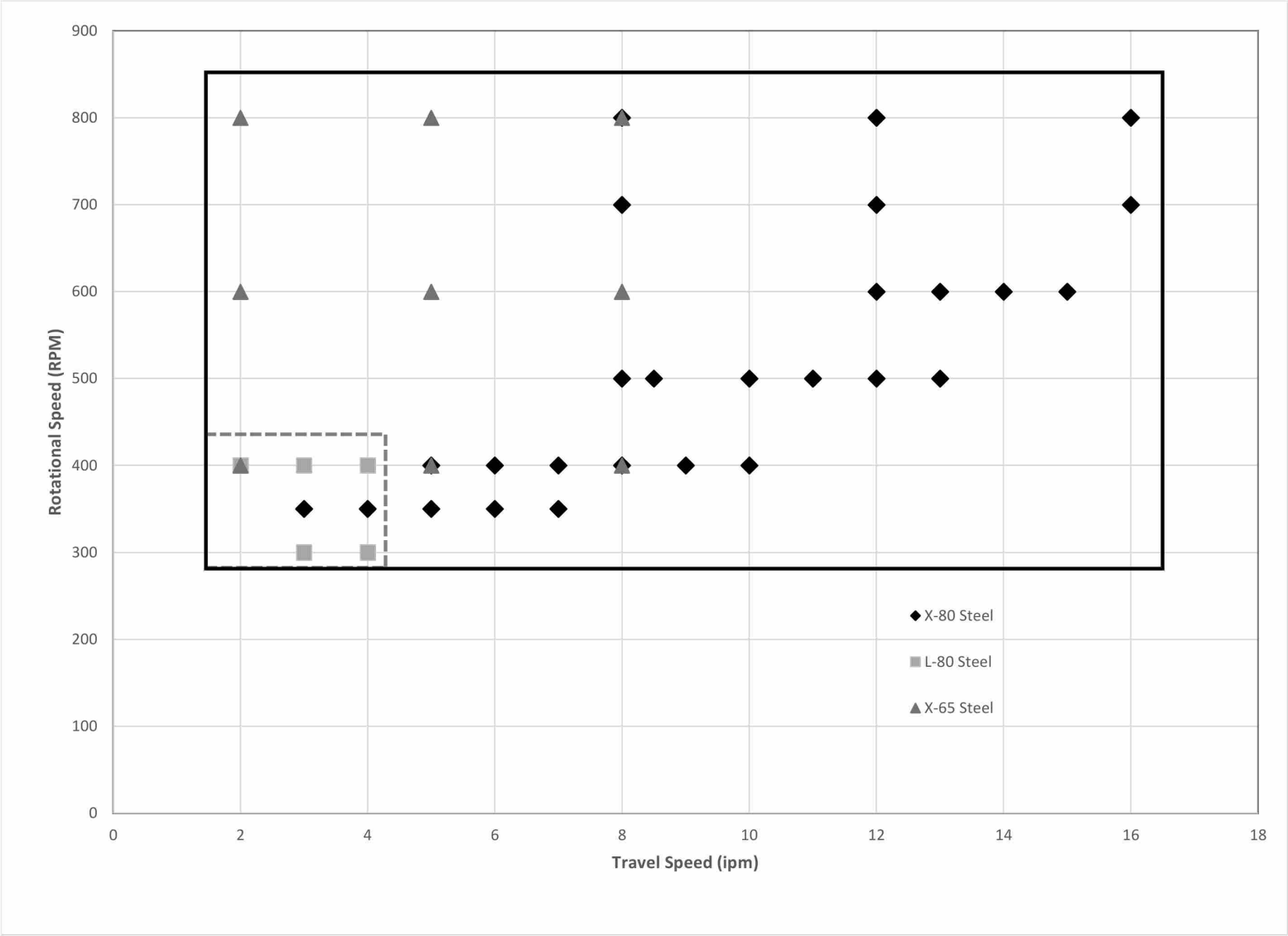

Figure 2.1: Parameters (travel speed and tool rotation) used during preliminary study that resulted in quality welds for three of the preliminary alloys.

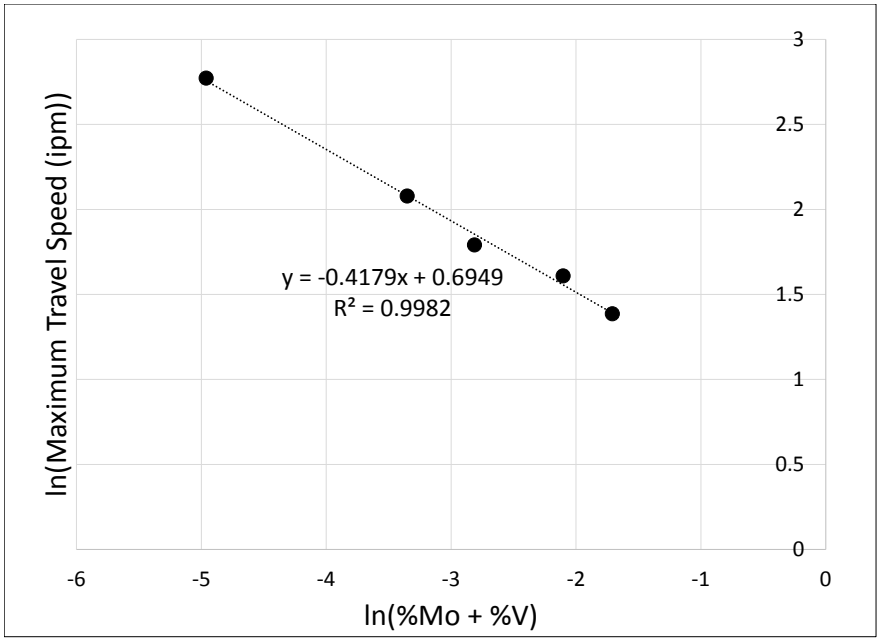

Figure 2.2: The natural log of both max travel speed and %Mo + %V content for each heat show a linear relationship.

CHAPTER 3. PROCEDURE

The purpose of this study was to explore the relationship between the high temperature properties and the friction stir weldability of HSLA steels. To do so, we needed to gain an adequate understanding of the high temperature properties of HSLA steels, and of their friction stir weldability. To gain this understanding, specialty heats of HSLA steel with known compositions were made and tested as described in this section.

3.1 Material

Based on the preliminary research, and our hypothesis that the friction stir weldability of an alloy of HSLA steel is tied to that alloy's high temperature properties, it was decided to focus our study on the effects of molybdenum, vanadium, niobium, and titanium. In order to test the effects of these elements on the properties in question, a half-factorial design of experiments was chosen, with the levels of the four elements varied between different heats of HSLA steel. The chemical compositions of the eight heats can be found in Table 3.1.

3.1.1 Design of Experiments

A half factorial (2^{4-1}) design was chosen for the study. This allowed us to determine the main effects of all four micro-alloying elements with only eight heats of steel, instead of the sixteen that would be required in a full factorial (2^4) design.

In a half factorial design, a subset (half) of the original number of variable combinations is chosen to be run. The subset chosen for our experiment can be seen in Table 3.1. The subset of runs is chosen based on what level of accuracy is desired. With this design, we can accurately estimate the main effects of the elements in the study, as they are not confounded with two-way interactions. In the design, two-way interactions are confounded with other two-way interactions, but, for the purposes of this study, the main effects are sufficient.

Table 3.1: This table lists the chemical composition of the 8 HSLA steel heats used. The highlighted portion show the elements varied between the heats,with the darker gray showing the high values, and white showing the low values.

Heat #	**Description**	**C**	**Si**	**Mn**	**P**	**S**	**Al**	**Mo**	**Nb**	**V**	**Ti**	**N**	**O**
189	High: Mo-Nb-V-Ti	0.065	0.226	1.37	0.011	0.0022	0.018	0.300	0.101	0.099	0.045	0.0040	0.0025
186	High: V-Ti Low: Mo-V	0.065	0.203	1.43	0.012	0.0019	0.019	0.004	0.003	0.102	0.049	0.0040	0.0012
188	High: Mo-Ti Low: Nb-V	0.067	0.200	1.37	0.010	0.0023	0.018	0.298	0.002	0.003	0.050	0.0044	0.0019
184	High: Nb-Ti Low: Mo-V	0.064	0.203	1.44	0.011	0.0020	0.019	0.002	0.104	0.002	0.051	0.0045	0.0010
183	High: Mo-V Low: Nb-Ti	0.068	0.205	1.44	0.012	0.0017	0.018	0.303	0.002	0.101	0.001	0.0041	0.0008
182	High: Nb-V Low: Mo-Ti	0.066	0.214	1.40	0.017	0.0019	0.021	0.005	0.109	0.099	0.003	0.0043	0.0008
187	High: Mo-Nb Low: V-Ti	0.062	0.209	1.38	0.011	0.0018	0.019	0.302	0.100	0.001	0.002	0.0036	0.0010
185	Low: Mo-Nb-V-Ti	0.064	0.209	1.43	0.014	0.0020	0.016	0.002	0.003	0.002	0.001	0.0045	0.0017

3.2 Determining High Temperature Properties

Samples for testing high temperature properties were cut by wire EDM from the base metal of each heat. All cylindrical samples were 0.48 inches in length and diameter. The longitudinal axis of the samples was perpendicular to the rolling direction of the material, along the thickness of the material.

Hot compression tests on the heats were performed using a Gleeble 3500 system. Samples were placed between the compression anvils of the Gleeble system. Thermocouples were attached to both ends of the sample to measure the temperature of the cylinder. The specimen was then heated to the testing temperature and crushed at a constant strain rate of 5 s^{-1} until the total engineering strain was 30%. A picture of the gleeble testing specimens, pre and post testing, can be seen in Figure 3.1. Each heat was tested at three different temperatures: 950 °C, 1000 °C, and 1100 °C.

Figure 3.1: Picture of two high temperature compression test samples. The one on the left has not been tested. The right sample has been compressed 30% as part of the hot temperature compression test.

3.3 Determining Friction Stir Weldability

To determine the friction stir weldability of each heat, bead-on-plate welds were run at increasing feed rates until defects were observed during analysis of the weld. The highest feed rate at which a defect free weld can be run is considered the friction stir weldability of the heat.

3.3.1 Welds

Welds in this study were run using a MTI model RM2 FSW machine with a polycrystalline cubic boron nitride (PCBN) CS4 tool (model E44111, see Appendix A for the tool drawing). Each plate was first ground on both sides to remove mill scale, leaving a clean surface for welding.

Due to the length of the plates (9 in), welds were kept to a length of 7 in. In order to conserve material, each weld was used to test three separate travel speeds. The first inch was used to ramp up to the first testing travel speed, allowing the material to heat to a temperature of about 800 °C. The rest of the weld was broken into three 2 inch segments, each at an increasing travel speed. The tool was plunged to a depth of 0.215 inches while rotating at 450 RPM. During the ramp up portion of the weld, the spindle was rotated at 600 RPM to cause additional frictional heating. The spindle rotation was held at 450 RPM during the main weld phase. The depth of the weld was held to 0.215 inches for the duration of the weld.

3.3.2 Analysis of Welds

For every weld, a metallographic sample was cut out of each distinct travel speed zone using a water jet. These samples were mounted in a bakelite fixture and polished to a 1 μm finish, and then etched with a 2% nital solution. The polished sample was then examined by optical microscopy for defects in the weld area caused by a lack of consolidation. An example of the defect looked for can be seen in Figure 3.2 on page 13.

If a defect was not found, another weld was run at higher travel rates. If a defect was found, additional welds were run at lower feed rates to attempt to pinpoint the speed at which defects first appear. These welds were run as described in Section 3.3.1.

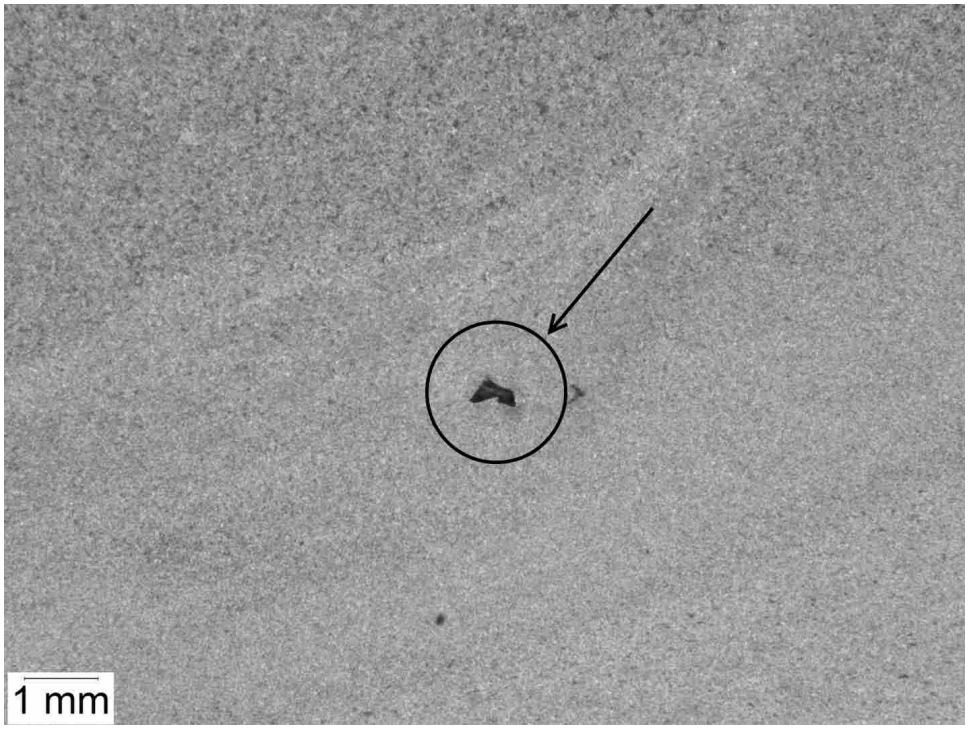

Figure 3.2: Example of a worm-hole defect. This weld was run at 7 inches per minute in Heat 183.

3.3.3 Analysis of Weld Forces

Weld data, including travel speed, forces in the x, y, and z directions, and spindle torque, were recorded by the friction stir welding machine. These data points were recorded several times a second for later analysis.

After welding was completed, the data records for each weld were examined to identify relationships between the weld forces and weld quality, travel speed, and high temperature properties of HSLA steels.

CHAPTER 4. RESULTS AND DISCUSSION

4.1 High Temperature Properties

The high temperature properties of the HSLA alloys used in the preliminary study are not known. In order to test for correlation between the preliminary study's alloys' friction stir weldability and their high temperature properties, these properties must first be estimated.

In order to estimate these properties for the preliminary heats, we used the results from our Gleeble high temperature compression tests to create linear equations based on the high temperature properties in question. These linear equations accurately predict high temperature yield stress, maximum stress, and hardening rate constant as a function of alloying composition and temperature over the ranges examined in this study.

4.1.1 Gleeble Specimen Analysis

Before analyzing the Gleeble data, we examined the tested specimens to assess the quality of the results.

The ideal cylindrical compression sample deforms uniformly through the thickness of the sample. As the height is compressed, the diameter at every point along the thickness should expand the same amount. Because of friction at the clamping ends, all real compression samples experience barreling, where the diameter away from the clamping ends expands more than the diameter at the ends. Barreling is illustrated in Figure 4.1. Percent barreling is calculated by Equation 4.1, where D_{max} is the maximum diameter of a sample crushed to a height h_c, and h_o and D_o are the original height and diameter of the sample [17]:

$$\%Barreling = (\frac{h_c(D_{max})^2}{h_o(D_o)^2} - 1) * 100 \tag{4.1}$$

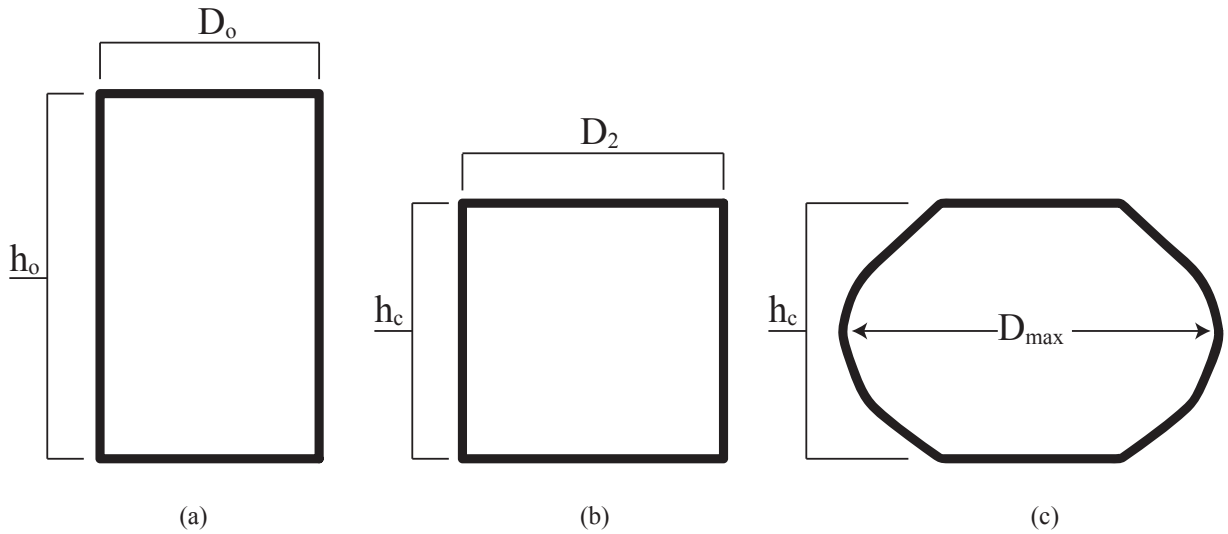

Figure 4.1: Diagrams of samples (side view) illustrating (a) Uncrushed sample. (b) Crushed sample with zero barreling. (c) Crushed sample with exaggerated barreling.

Barreling is only of concern in compression testing if the deformation from ideal is 10% or more [18]. Analysis of our samples reveals an average percent barreling of 4.51%, with a standard deviation of 0.91%. The maximum barreling on any sample is 6.95%. Because of this, barreling is not a concern in our experiments or in the analysis of our compression test data.

Another potential source of error to be addressed is the ovality of the crushed sample, or the degree to which the specimen is out of round. Ovality is illustrated in Figure 4.2. Ovality can be calculated by Equation 4.2, where "a" is the maximum diameter of a face, and "b" is the minimum diameter:

$$\%Ovality = \frac{2(a-b)}{a+b} * 100 \tag{4.2}$$

Analysis of our specimens show an average percent ovality of 0.42%, with a standard deviation of 0.36%. The maximum ovality on any sample is 1.36%. No standards for ovality in high temperature compression testing could be found, but ovality is not a concern in our study, due to the low magnitude of ovality observed.

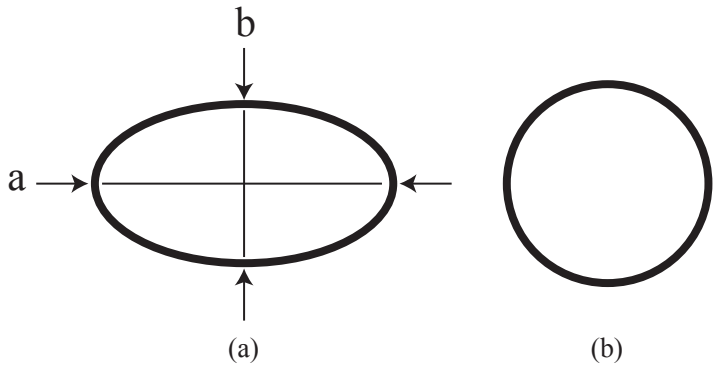

Figure 4.2: Top view of samples (a) Diagram of an out of round sample, with "a" representing the large axis, and "b" the small axis of the oval. (b) An oval with an ovality of 1.36%, which is the maximum for any of our samples.

4.1.2 Gleeble Data Analysis

The Gleeble 3500 system used for hot compression testing recorded time, force, engineering strain, anvil head position, and the temperature at both ends of the specimen.

Strain Rate

From the strain and time data, strain rate was calculated to ensure uniformity of strain rate between the samples. The average strain rate for the samples was $5.17s^{-1}$ with a standard deviation of $0.05s^{-1}$. The low standard deviation of the strain rates aided in arriving at accurate results derived from the gleeble compression test data. The high precision and accuracy of the strain rates is one indication that the compression tests were performed correctly.

True Stress and True Strain

True stress was calculated from the recorded force and instantaneous height, as measured by the anvil head position, using Equation 4.3, where F_x and h_x represent the force and the height of the sample at that instant, and r_o and h_o represent the original radius and height of the sample being crushed [19]:

$$\sigma_t = \frac{F_x h_x}{\pi r_o^2 h_o} \tag{4.3}$$

True strain was calculated from the instantaneous height (h_x) and the original height (h_o), using Equation 4.4 [19]:

$$\varepsilon_t = ln(\frac{h_o}{h_x}) \tag{4.4}$$

To account for play in the testing apparatus, displacement values were adjusted so that a line extrapolated downward from the elastic portion of the true stress - true strain curve intersects with the origin.

Figure 4.3 shows the true stress vs true strain chart for the sample of Heat 182 run at 950 °C.

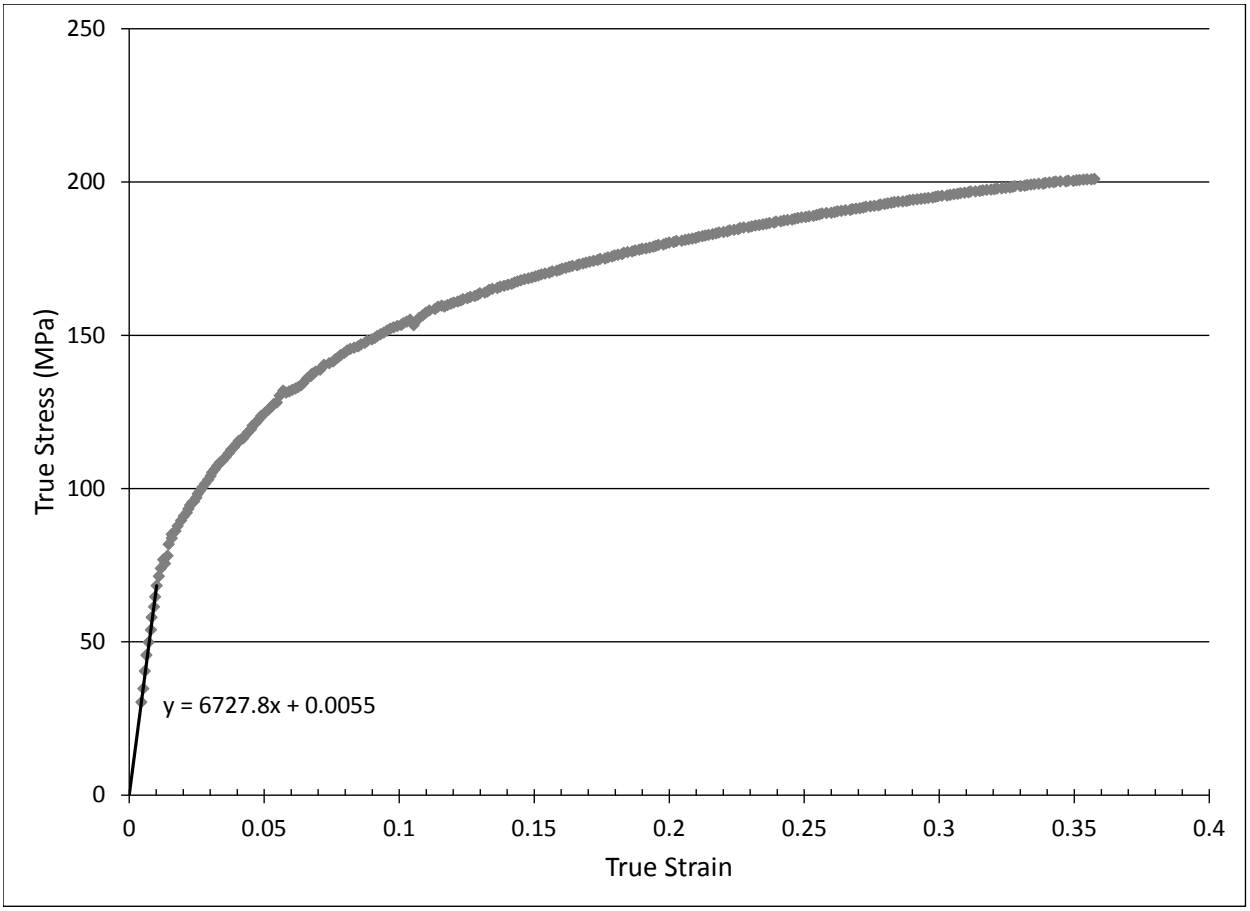

Figure 4.3: True stress - true strain chart for the sample of Heat 182 run at 950 °C. The slope of the equation on the left was used to estimate the yield stress of the material.

To estimate yield strength, a line with the same slope as the elastic portion of the true stress - true strain curve was drawn from $\varepsilon_t = 0.002$ upward until it intersected with the curve.

The maximum true stress, σ_m, reached in each compression test was also recorded and analyzed.

In order to compare strain hardening rates between the different heats and testing temperatures, strain hardening rate constants (θ_0) were calculated for each specimen [20]. This was done by graphing the hardening rate (θ) as a function of true stress (σ_t), and then extrapolating the slope of the Stage III hardening backwards to where it intercepts the hardening rate axis. This value is the strain hardening rate constant for that heat at that testing temperature. This constant is known to vary with testing temperature [20]. Figure 4.4 illustrates the process used for determining the strain hardening rate constant (θ_0). The hardening rate, being a derivative of stress as a function of strain, required some filtering to smooth the data enough to be usable. A total variation algorithm [21] was used to filter the data.

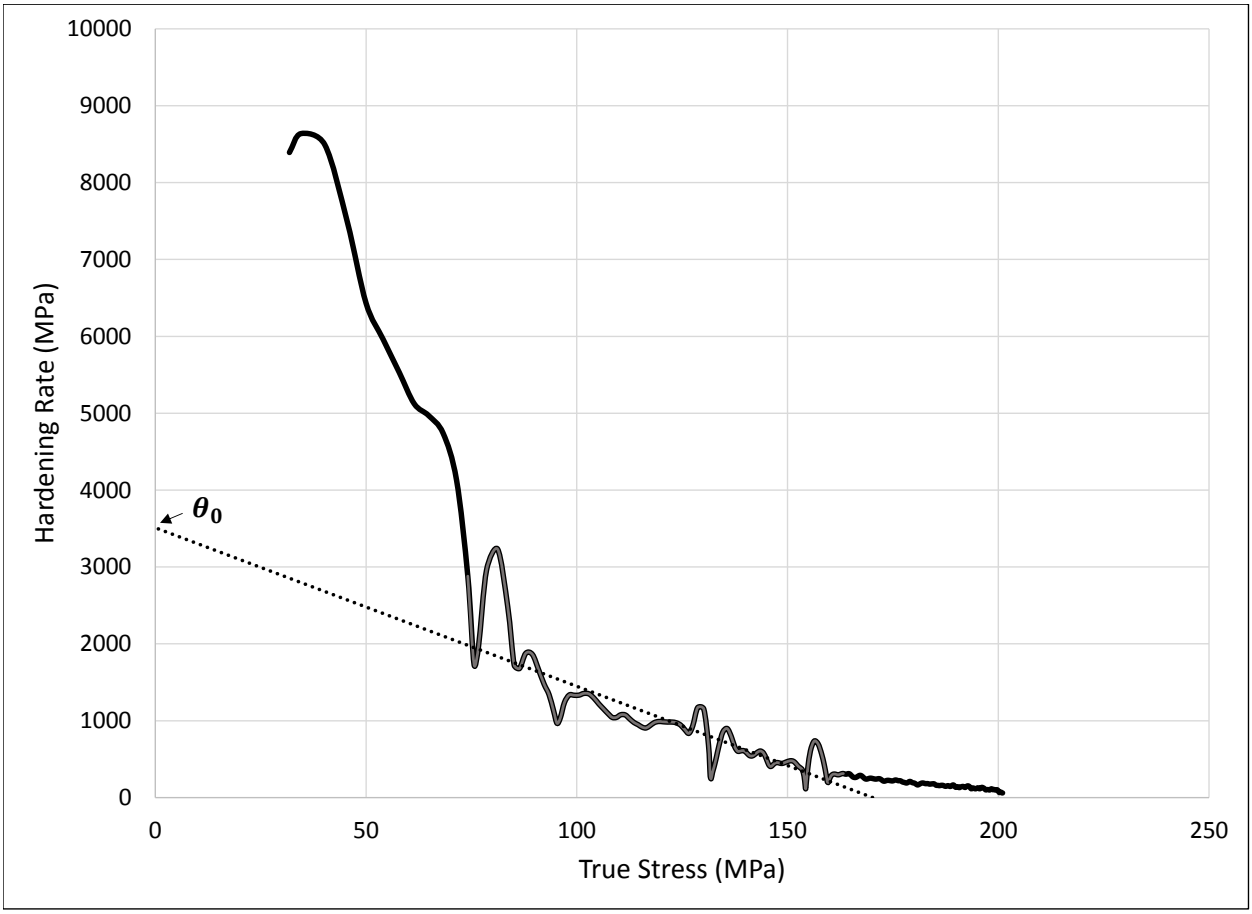

Figure 4.4: Strain hardening rate graphed versus true stress, showing the line drawn through the strain hardening rate curve used to estimate the strain hardening rate constant.

The yield stress, strain hardening rate constant, and maximum true stress obtained for each of the specimens can be seen in Table 4.1 and in Figure 4.5. Table 4.1 also notes the relative composition levels used in the experimental heats. In this notation, a '+' symbol indicates the high value of the composition level, and '-' indicates the low value. These high and low values are used to calculate effects, as shown in section 4.1.3.

Table 4.1: Yield stress (σ_y), strain hardening rate constant (Θ_0), and maximum true stress (σ_t) of the 8 experimental heats at the elevated testing temperatures.

	Composition Levels				**σ_y (MPa)**			**Θ_0 (MPa)**			**σ_t (MPa)**		
Heat	**Mo**	**V**	**Nb**	**Ti**	**950 °C**	**1000 °C**	**1100 °C**	**950 °C**	**1000 °C**	**1100 °C**	**950 °C**	**1000 °C**	**1100 °C**
182	-	+	+	-	80	77	54.6	3510.4	3206.1	2531	201.03	179.56	141.41
183	+	-	+	-	54	46.5	41	2780.2	2491	1851.9	193.09	171.82	131.66
184	-	+	-	+	73.5	69.2	47	3183.7	2922.8	2528.5	196.12	177.71	138.32
185	-	-	-	-	50.4	40	38.1	2530	2451.9	1758	178.11	160.32	121.72
186	-	-	+	+	68	50.8	38.4	3033.1	2877.4	2342	191.29	171.51	132.25
187	+	+	-	-	81.4	66.7	52.4	3739.8	3688.1	2749.5	205.22	184.57	143.17
188	+	-	-	+	75	59.5	41	3084	2915.4	2383.8	200.12	176.05	137.68
189	+	+	+	+	79.5	74.2	56.8	4499.2	4327.9	3613	206.68	187.95	144.61

4.1.3 Linear Model

In order to estimate yield stress, maximum stress, and hardening rate constants for HSLA steels as a function of chemical composition and elevated testing temperature, we analyzed the data from our 950 °C and 1100 °C runs, and treated both together as a $2 * 2^{4-1}$ design. The two halves of the design are identical, but use different testing temperatures. This allowed us to estimate the effects of the four alloying elements and also the effect of temperature on the physical property being examined. Because of the half factorial nature of this design, some confounding of two factor interactions with other two factor interactions occurred. The full statistical model, with results and statistical values, can be found in Appendix D.

From the analysis of each physical property, linear models of the following form were created:

$$Y = \alpha_0 + \sum(\alpha_i - 2\sum_{j \neq i} \alpha_{ij}\bar{x}_j)X_i + 2\sum_{j \neq i} \alpha_{ij}X_iX_j \tag{4.5}$$

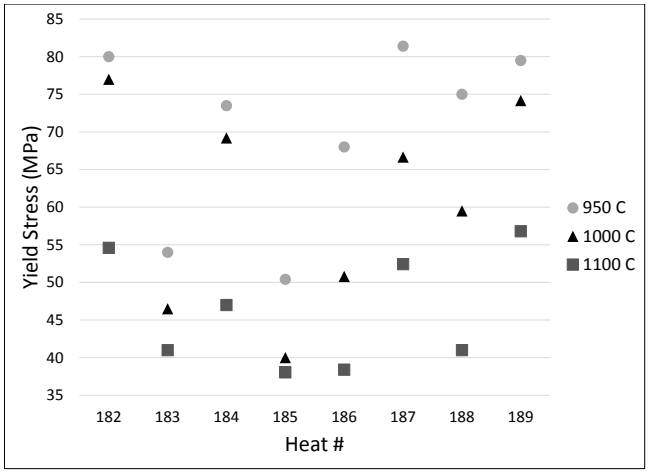

(a) Yield Stress

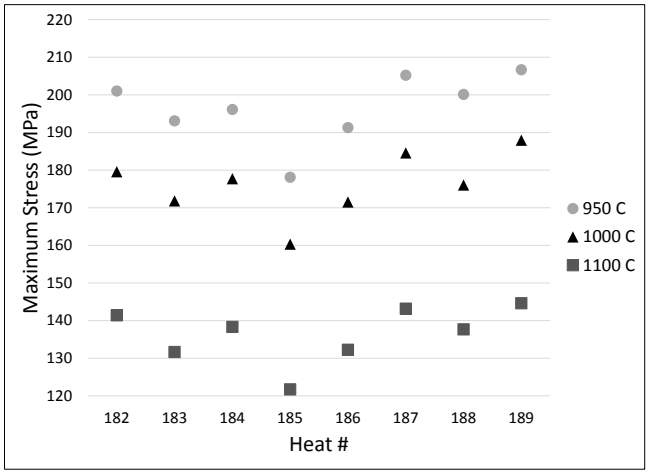

(b) Maximum Stress

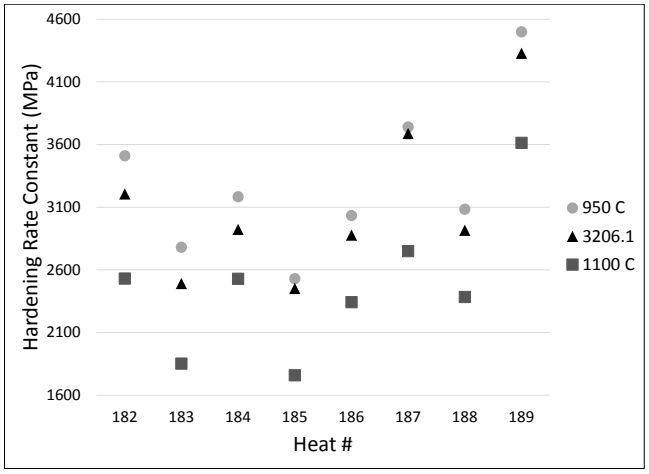

(c) Hardening Rate

Figure 4.5: High temperature properties of experimental heats.

where Y = the estimated value of the physical property, and X_i = the component amount. For example: Molybdenum concentration (%), or temperature (K). The remaining terms are explained below.

$$\alpha_0 = \overline{Y} - \sum_{i=1}^{5} \frac{\beta_i}{2} \frac{\overline{x}_i}{r_i} - \sum_{i=1}^{4} \sum_{j=i+1}^{5} \frac{\beta_{ij}}{4} \frac{\overline{x}_i \overline{x}_j}{r_i r_j} \tag{4.6}$$

where $\overline{Y}$ = the average property value of the tests used in analysis, β_i and β_{ij} = the main and interaction coefficients, $\overline{x}_i$ and r_i = the average and range of the minimum and maximum values used in the study for that variable.

$$\alpha_i = \frac{2\beta_i}{r_i} \tag{4.7}$$

$$\alpha_{ij} = \frac{\beta_{ij}}{r_i r_j} \tag{4.8}$$

The effect of a variable (E_i) on the value of the property is defined as:

$$E_i = \overline{Y_H} - \overline{Y_L} \tag{4.9}$$

where $\overline{Y_H}$ and $\overline{Y_L}$ are the means, at high and low variable levels, of the physical values in question.

To determine the main factor coefficients (β_i) of the components, the following formula was used:

$$\beta_i = \frac{E_i}{2} \tag{4.10}$$

where $\overline{Y_H}$ and $\overline{Y_L}$ are the means, at high and low variable levels, of the physical values in question. The coefficient is one half the effect of the variable.

For example, to determine the coefficient of molybdenum on yield stress, the following equation would be used:

$$\beta_{Mo} = \frac{\frac{(54+81.4+75+79.5+41+52.4+41+56.8)}{8} - \frac{(80+73.5+50.4+68+54.6+47+38.1+38.4)}{8}}{2} = 1.95 \tag{4.11}$$

The first fraction (54+81.4+...) contains yield stress values at 950 °Cand 1100 °Cthat had a high value of molybdenum, while the second fraction (80+73.5+...) contained the values from heats with the low value of molybdenum. This allowed us to determine the effect of increasing molybdenum content on yield stress.

The coefficients of molybdenum, niobium, vanadium, titanium, and testing temperature on yield stress, maximum stress, and hardening rate are listed in table 4.2.

Table 4.2: Coefficients of the 4 alloying elements and testing temperature on yield stress, maximum stress, and hardening rate.

	Molybdenum	**Niobium**	**Vanadium**	**Titanium**	**Temperature**	**Mean Value**
Yield Stress	1.95	7.46	0.85	1.71	-12.03	58.19
Maximum Stress	3.87	5.67	27.50	1.98	-30.05	166.40
Hardening Rate	205.31	412.03	137.74	201.05	-412.65	2882.4

Because this is a half factorial design, secondary interaction effects are confounded with other secondary interaction effects, according to the confounding rule used to design the experiment.

The confounding rules for this design are:

Ti = Mo*Nb*V

V*Ti = Mo*Nb

Mo*Ti = Nb*V

Nb*Ti = Mo*V

Because of this confounding, it is not possible to be certain which interactions in an interaction pair are significant. When choosing between two confounded interactions, the interaction with the largest parent main effects was used in our linear models as the interaction. It should be noted, however, that additional study is needed to explore and confirm these interactions in the linear models.

The interaction coefficients were determined in the same manner as the main factor coefficients, using equation 4.10. They can be seen in table 4.3.

The main effects and two factor interactions are shown in Figures 4.6, 4.7, and 4.8.

Table 4.3: Coefficients of the two factor interactions for yield stress, maximum stress, and hardening rate constant.

	Mo*Ti or Nb*V	Nb*Ti or Mo*V	V*Ti or Mo*Nb	Temp*Mo	Temp*Nb	Temp*V	Temp*Ti
Yield Stress	1.23	-3.16	-0.07	-0.30	-0.92	0.70	-2.07
Maximum Stress	-2.32	-1.34	-1.05	1.66	1.36	1.37	2.70
Hardening Rate	106.31	-39.30	150.71	-25.44	-26.94	-26.20	46.1

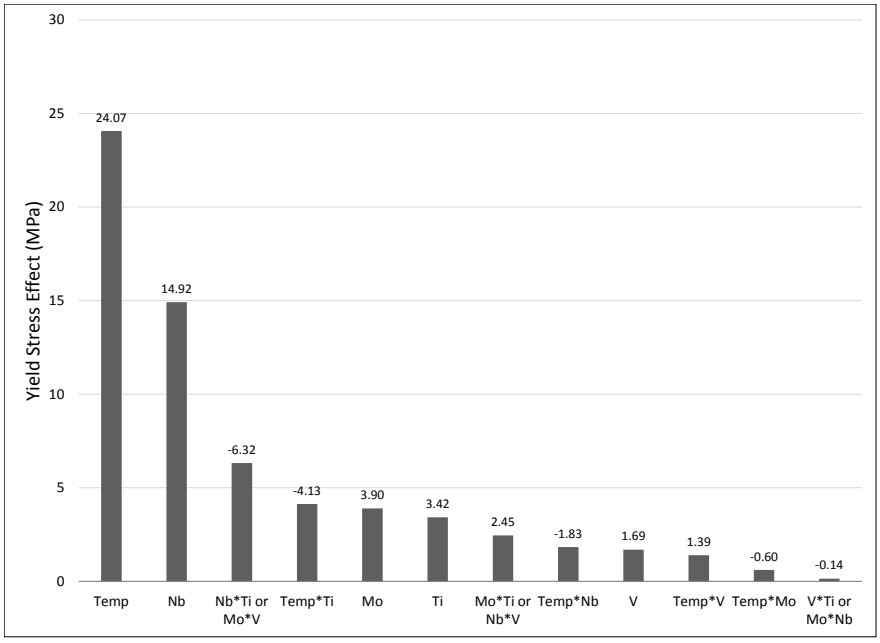

Figure 4.6: The main effects and two factor interactions for yield stress.

The terms used in our linear models were chosen based on Adjusted R^2 values using stepwise regression [22]. The terms used are:

For Yield Stress:	Mo, Nb, Ti, Temp, Nb*Ti, and Temp*Ti
For Maximum Stress:	Mo, Nb, V, Ti, Temp, and Nb*Ti
For Hardening Rate:	Mo, Nb, V, Ti, Temp, Mo*Nb, and Mo*Ti

The linear equations to predict yield stress (σ_y), maximum stress (σ_m), and hardening rate constants (θ_0) in HSLA steels are:

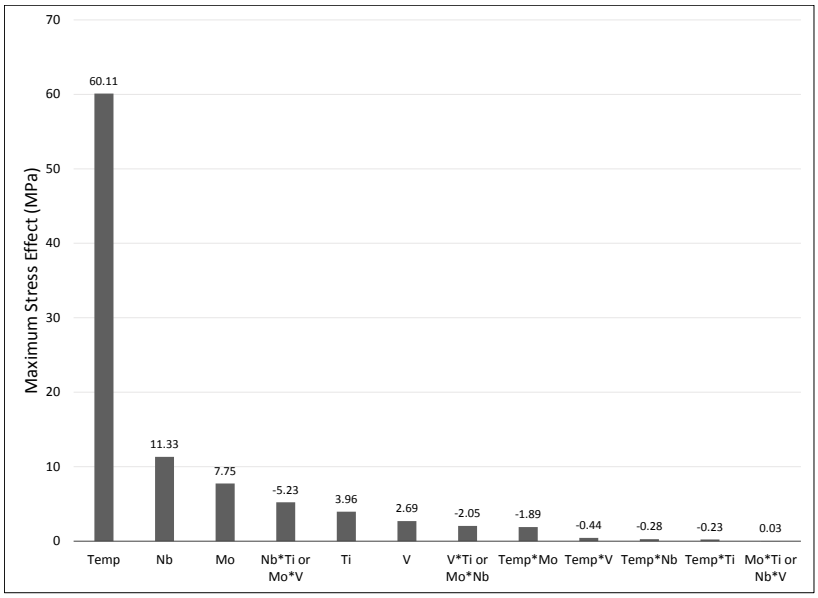

Figure 4.7: The main effects and two factor interactions for maximum stress.

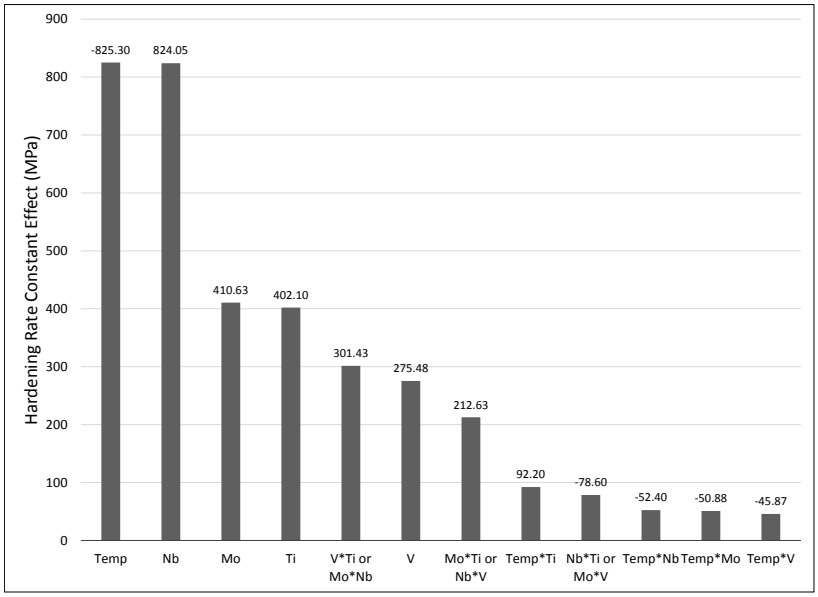

Figure 4.8: The main effects and two factor interactions for hardening rate constants.

$$\sigma_y = 214.2808 + 13.1145(Mo\%) + 219.3935(Nb\%) + 1663.7985(Ti\%) - 0.1318(Temp(K)) - 2633.2778(Nb\%)(Ti\%) - 1.1245(Temp(K))(Ti\%) \quad (4.12)$$

$$\sigma_m = 670.4320 + 26.0869(Mo\%) + 171.1843(Nb\%) + 27.4968(V\%) + 214.2808(Ti\%) - 0.4007(Temp(K)) - 2179.1702(Nb\%)(Ti\%) \quad (4.13)$$

$$\theta_0 = 9296.0054 - 418.8776(Mo\%) + 5270.7715(Nb\%) + 2810.9694(V\%) + 3779.1744(Ti\%) - 5.4937(Temp(K)) + 20712.2243(Mo\%)(Nb\%) + 29220.7722(Mo\%)(Ti\%) \quad (4.14)$$

These equations show the relationship between the four alloying elements and temperature with the high temperature properties examined. The relative size of the coefficient before each term indicates the importance of that term to the high temperature property. For example, for yield stress the most important terms are titanium (with a coefficient of 1663.8), and niobium (with a coefficient of 219.4). In the preliminary study, it was discovered that molybdenum and vanadium content influence the friction stir weldability of HSLA steels. If there is a link between friction stir weldability and high temperature properties of HSLA steels, it is reasonable to expect molybdenum and vanadium content to also be major factorts in determining the high temperature properties, but this is not what we see here. From these equations, we see that niobium and titanium, not molybdenum and vanadium, have the main effects on yield stress, maximum stress, and hardening rate constant. The relationship between high temperature properties and friction stir weldability is examined further in Section 4.3, but this is our first indication that our initial hypothesis is not correct.

The linear models' correlation with our observed results is very good for all three high temperature physical properties. For yield stress, the R^2 value is 0.9275. For maximum stress, the R^2 value is 0.9974. For the hardening rate constant, the R^2 value is 0.9774. These high R^2 values indicate that our linear models accurately predict the high temperature physical properties for our

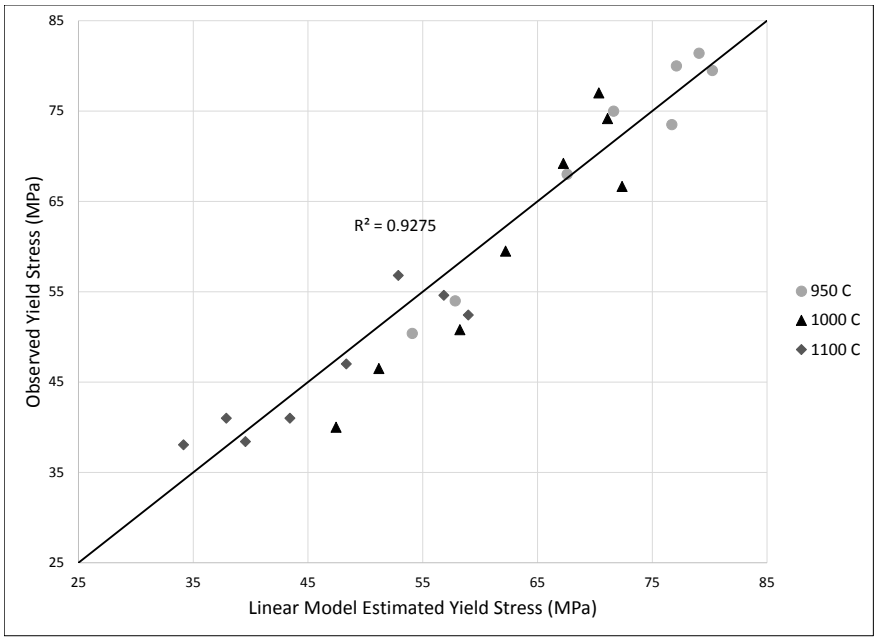

Figure 4.9: A comparison of the predicted yield stress, as determined using the linear model, with the observed yield stress. The diagonal line indicates where the predicted yield stress would equal the observed yield stress.

8 experimental heats. In order to determine if the models can predict properties for other HSLA heats, outside corroboration was required, as described below.

4.2 Medina Peak Stress Comparison

Medina and Hernandez, in a 1996 paper, developed a model to estimate peak stress in HSLA steels as a function of chemical composition, strain rate, and temperature [23]. They examined HSLA steels in similar compositional ranges as used in this study. Beyond the peak strain, at which peak stress was observed, dynamic recrystallization of the material lowered the observed stress. The maximum observed stress from our high temperature compression tests occurred in the same range of strain at which Medina observed peak stress. As can be seen in Figure 4.12 our maximum true stress correlates well with the predicted peak stress obtained with the Medina equations. Because of this, we are comfortable considering our measured maximum true stress the peak stress of the material at that strain rate and temperature.

To test our linear equations' ability to predict properties beyond our sample group of HSLA steels, we compared the maximum stresses for the experimental alloys predicted using our max-

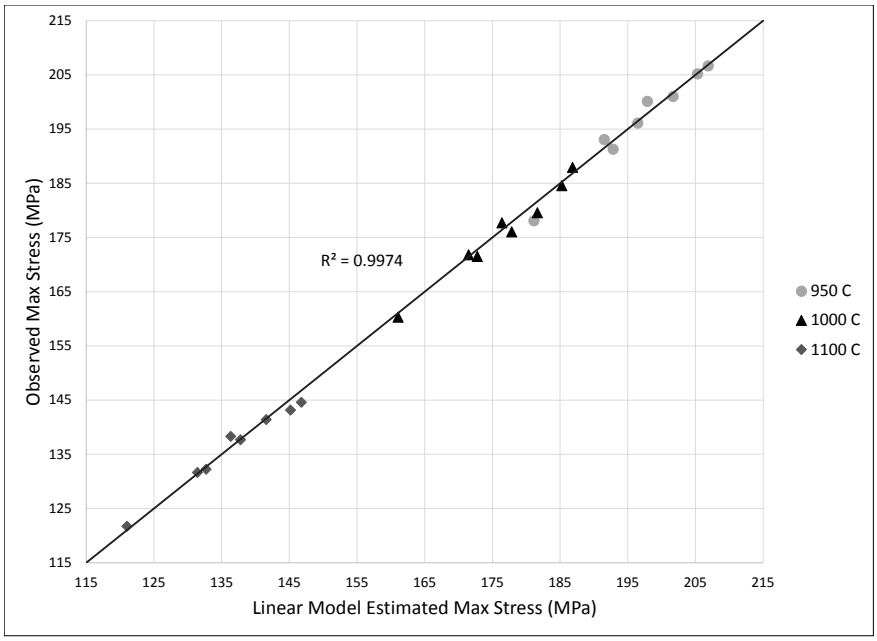

Figure 4.10: A comparison of the predicted maximum stress, as determined using the linear model, with the observed maximum stress. The diagonal line indicates where the predicted maximum stress would equal the observed maximum stress.

imum stress equation (Equation 4.13) to the maximum stresses obtained using the Medina equations [23]. The comparison was performed at our three testing temperatures (900 °C, 1000 °C, and 1100 °C). A graph of this comparison can be seen in Figure 4.13. The fit of this comparison is very good, with an R^2 value of 0.9882. This shows that our model produces the same results as an independently determined predictor of maximum stress.

This proves our model is a good predictor of maximum stress over the range of compositions and temperatures we examined. This indicates that our methodology for creating our linear model is correct, and our models for predicting yield stress and the hardening rate constant are also accurate over the range of compositions and temperatures we examined.

4.3 Friction Stir Weldability Correlations (Preliminary Heats)

Using the equations developed in Section 4.1.3 and the compositions listed in Table 2.1, high temperature physical properties for the five preliminary heats were estimated. These physical properties were used to test correlation between observed maximum travel speed (friction stir weldability) and the physical properties we studied.

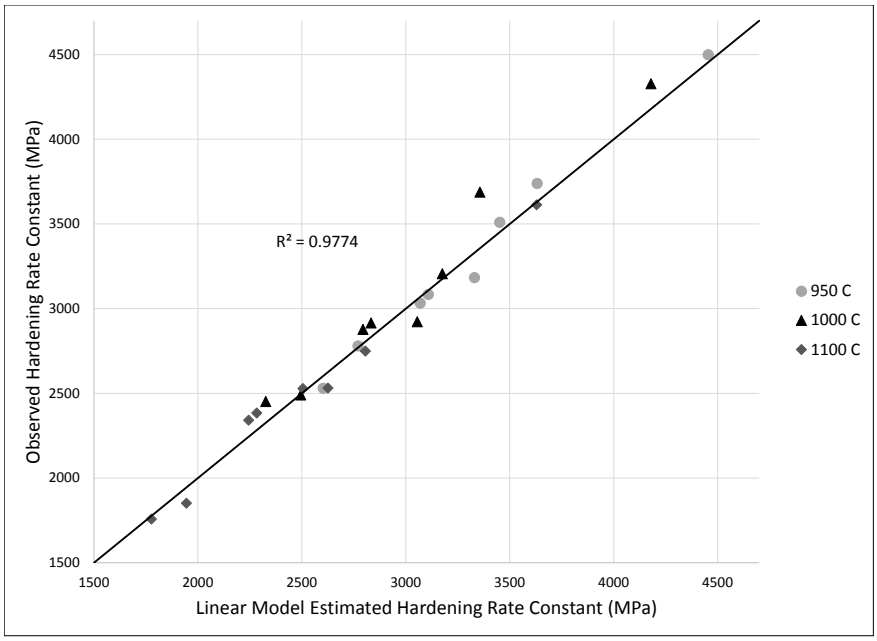

Figure 4.11: A comparison of the predicted hardening rate constant, as determined using the linear model, with the observed hardening rate. The diagonal line indicates where the predicted hardening rate constant would equal the observed hardening rate constant.

Our original hypothesis, after the preliminary study, was that there was a negative correlation between high temperature strength and maximum travel speed in HSLA steels. Comparison of the observed maximum travel speed and the predicted peak strength and yield strength of the preliminary heats shows that this is not the case. Instead, there is an apparent positive correlation between travel speed and high temperature strength, as seen in Figure 4.14 and in Figure 4.15.

There is also a positive correlation between maximum travel speed and hardening rate, as seen in Figure 4.16.

Temperature did not change the relationship between physical property and maximum travel speed, and so only the 1000 °C estimates are shown in these figures.

It was noted that the recorded friction stir weldability for X-80 is much higher than for the other heats. Because of this, it was decided to test the model to see if any one point was overly influencing the regression analysis. Cook's distance values, a measure of the influence a data point has on a regression model [24], were calculated for each point in the three models. Data points with Cook's distance values over 1 are considered highly influential [25]. For yield stress, maximum stress and hardening rate, the Cook's distance values for X-80 were 3.71, 3.21,

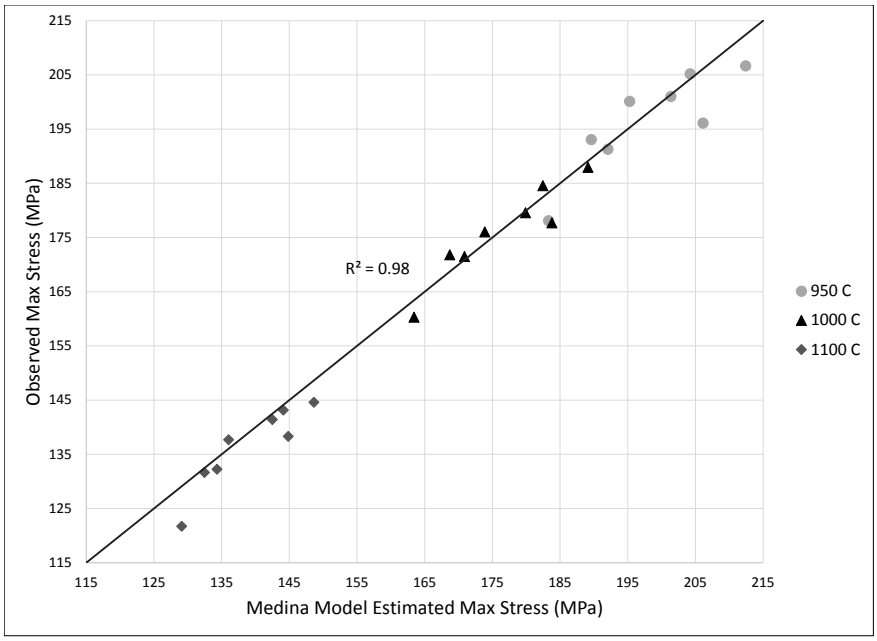

Figure 4.12: A comparison of the predicted peak stress, as determined using the Medina equations, with the observed maximum true stress. The diagonal line indicates where the predicted peak stress would equal the observed maximum true stress.

and 1.98 respectively. Consequently, we looked at correlations that both included and excluded X-80 to examine the effect of this influential point on the analysis. In both correlations, the general relationships discussed above hold true, although the relationship is more pronounced when X-80 is included, as is expected.

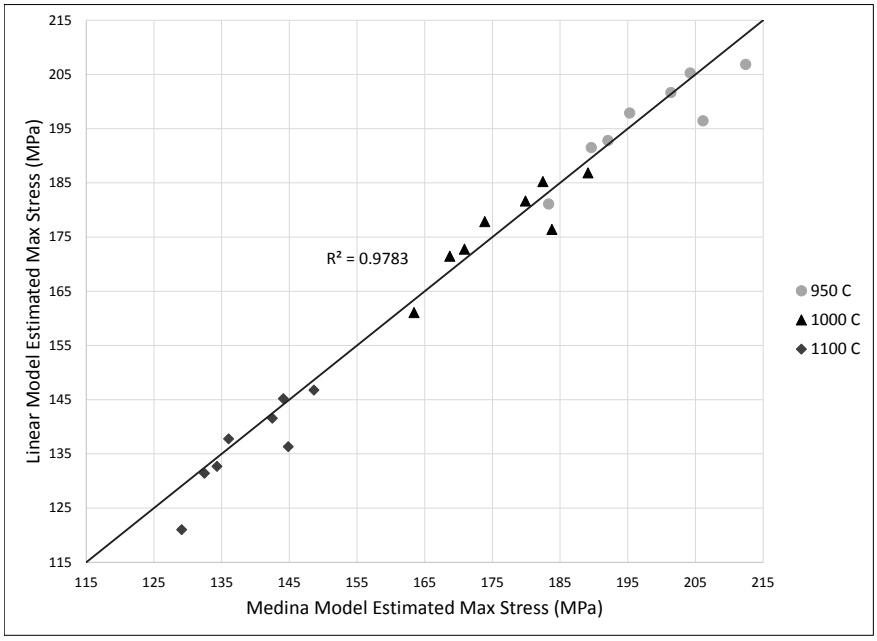

Figure 4.13: A comparison of the peak stress estimated using the Medina equations, with the maximum stress estimated by the linear equation. The diagonal line indicates where the predicted peak stress would equal the estimated maximum stress.

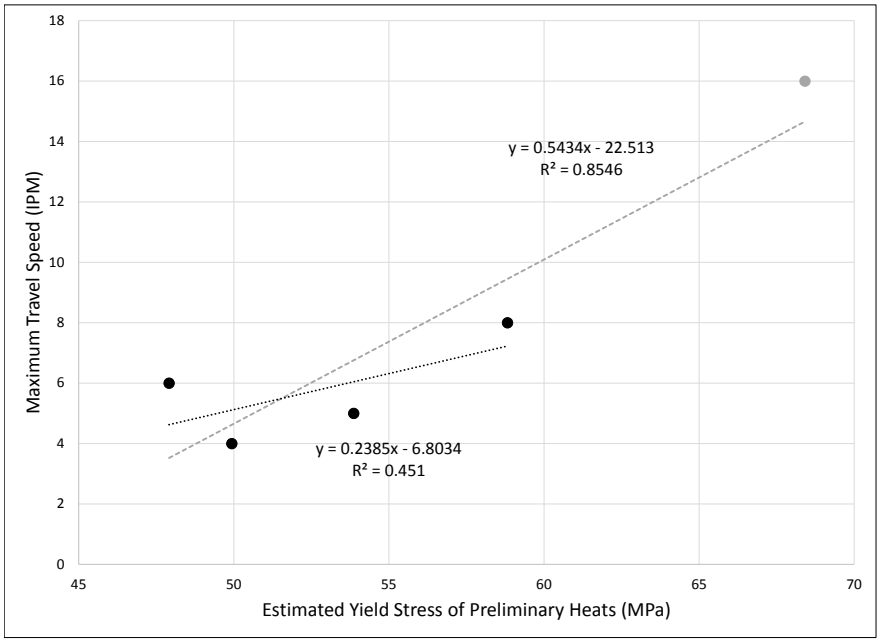

Figure 4.14: A comparison of observed maximum travel speed with predicted yield stress for the heats from the preliminary study. The predicted yield stresses were calculated for a testing temperature of 1000 °C.

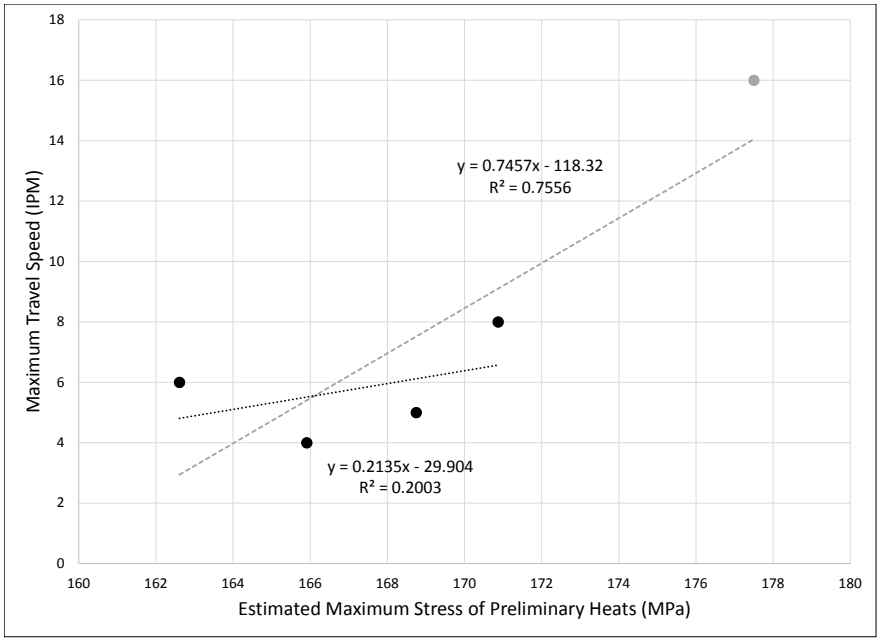

Figure 4.15: A comparison of observed maximum travel speed with predicted maximum stress for the heats from the preliminary study. The predicted maximum stresses were calculated for a testing temperature of 1000 °C.

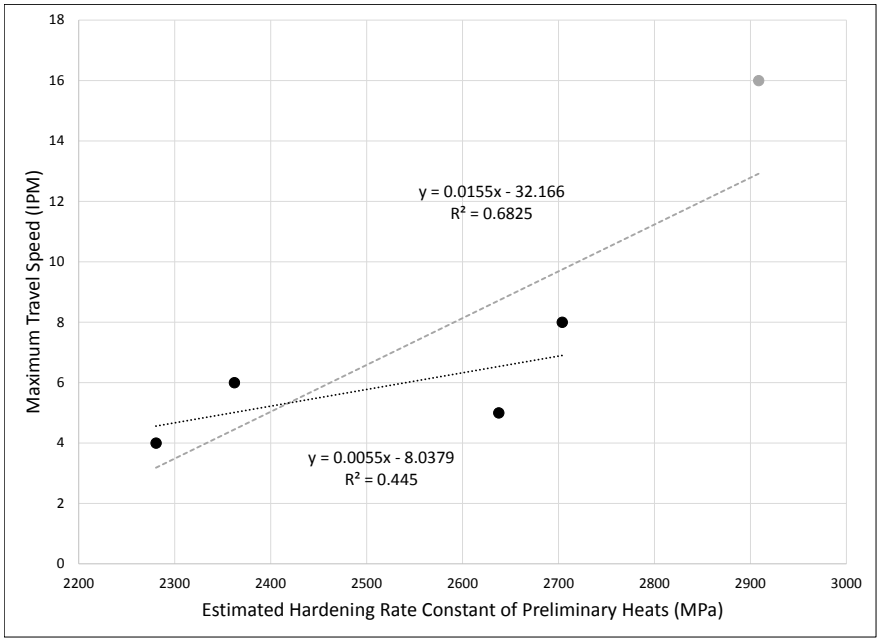

Figure 4.16: A comparison of observed maximum travel speed with predicted hardening rate constant for the heats from the preliminary study. The predicted hardening rate constants were calculated for a testing temperature of 1000 °C.

The fit for these correlations is poor. Examining the relationships with friction stir weldability, with out the effect of X-80, yield stress has an R^2 value of 0.451, maximum stress has an R^2 value of 0.2003, and the hardening rate constant has an R^2 value of 0.445.

The preliminary study, discussed in section 2.4, found a power law correlation between molybdenum and vanadium content and maximum travel speed in HSLA steels. This correlation can be seen in Figure 4.17. The power law correlation fits the observed friction stir weldability data much more closely than the high temperature property correlations examined in this study. The R^2 value for the correlation is 0.9982, which is more than double the R^2 for any of the high temperature property correlations examined.

These low R^2 values show a lack of relationship between these high temperature physical properties and friction stir weldability in HSLA steels. Like in the preliminary study, the only good correlation found is a power law relationship between molybdenum plus vanadium content and friction stir weldability. These results confirm that there is no relationship between high temperature properties and friction stir weldability. To attempt to further confirm these results, correlations with the friction stir weldability data of our experimental alloys were also examined.

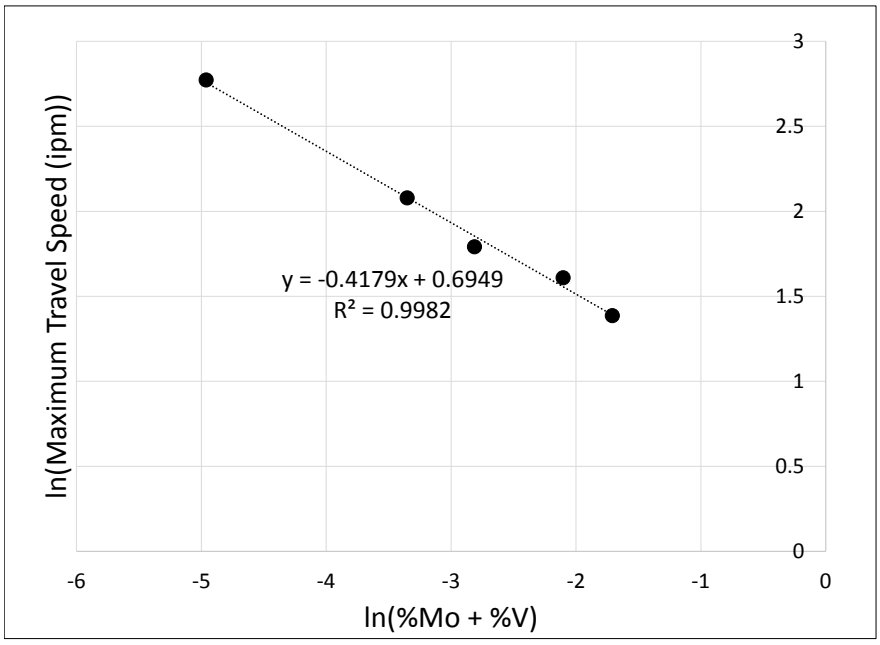

Figure 4.17: A log-log plot of maximum travel speed and %Mo + %V content for each heat that shows a linear relationship.

4.4 Friction Stir Weldability of Experimental Heats

Due to the experimental nature of the heats designed for this study, welding material was limited, narrowing the parameter scope we could examine to determining the friction stir weldability of each heat. As opposed to the process used to determine friction stir weldability in the preliminary study (see Section 2.4), which varied both travel speed and spindle speed, only travel speed was varied in our study due to the limited materials. In addition, there was not sufficient material to determine the friction stir weldability of heat # 185, as we ran out of material from that heat before a defect could be found. Further research with more materials is recommended to investigate the friction stir weldability trends highlighted by this study.

The travel speeds welded in each experimental heat are shown in Figure 4.18, along with the results of weld analysis for each segment. Based on the results of these welds, the friction stir weldability of each heat was estimated, as described in Section 3.3. The friction stir weldabilty of each heat is listed in Table 4.4.

Table 4.4: The maximum travel speed for each heat at which a good (defect free) weld was created during the course of the study. If no defect was discovered, as in the case of 185, "Not Determined" is put in the place of the friction stir weldability.

	Composition Levels				
Heat	Mo	V	Nb	Ti	Friction Stir Weldability (ipm)
182	-	+	+	-	6
183	+	-	+	-	5
184	-	+	-	+	9
185	-	-	-	-	Not Determined
186	-	-	+	+	6
187	+	+	-	-	9
188	+	-	-	+	6
189	+	+	+	+	5

Due to difficulties in welding the small plates available, the friction stir weldability values listed in Table 4.4 should be viewed as the lower bounds of the friction stir weldabilities for each experimental heat. The values are at least this high, but may actually be higher. The difficulties experienced in determining the friction stir weldabilities of the experimental steels are further described in Section 4.7.

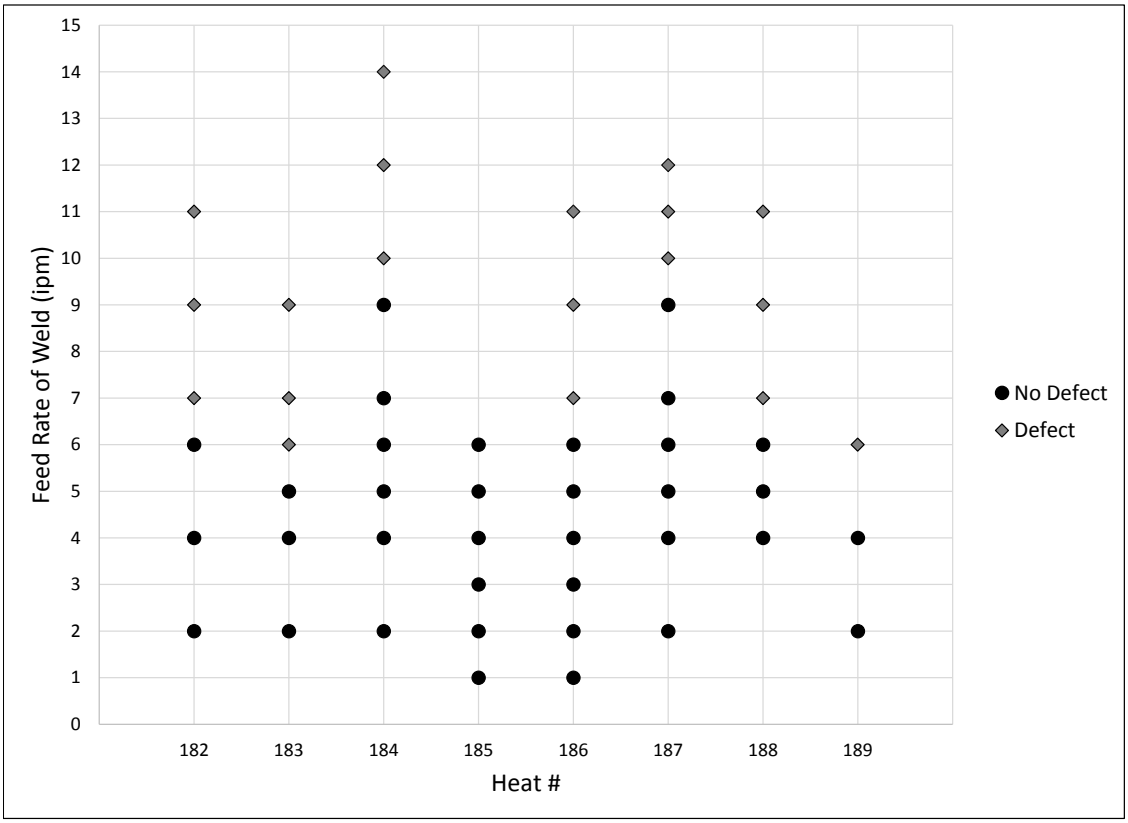

Figure 4.18: The feed rates (travel speeds) tried in each experimental heat, with the result of the weld.

4.5 Friction Stir Weldability Correlations (Experimental Heats)

To further test the original hypothesis, we examined the relationship between the experimental heats' measured high temperature physical properties and their determined friction stir weldability. Because no friction stir weldability could be determined for heat # 185, only seven heats were utilized in the analysis. The friction stir weldability of the experimental heats was compared with the heats' observed yield stress, maximum stress, and hardening rate constant. These correlations can be seen in Figures 4.19, 4.20, 4.21. The relationship between these heats' friction stir weldability and their molybdenum and vanadium contents was also examined. This correlation can be seen in Figure 4.22. This relationship was examined because the preliminary research showed a strong power law relationship between the molybdenum plus vanadium content and friction stir weldability.

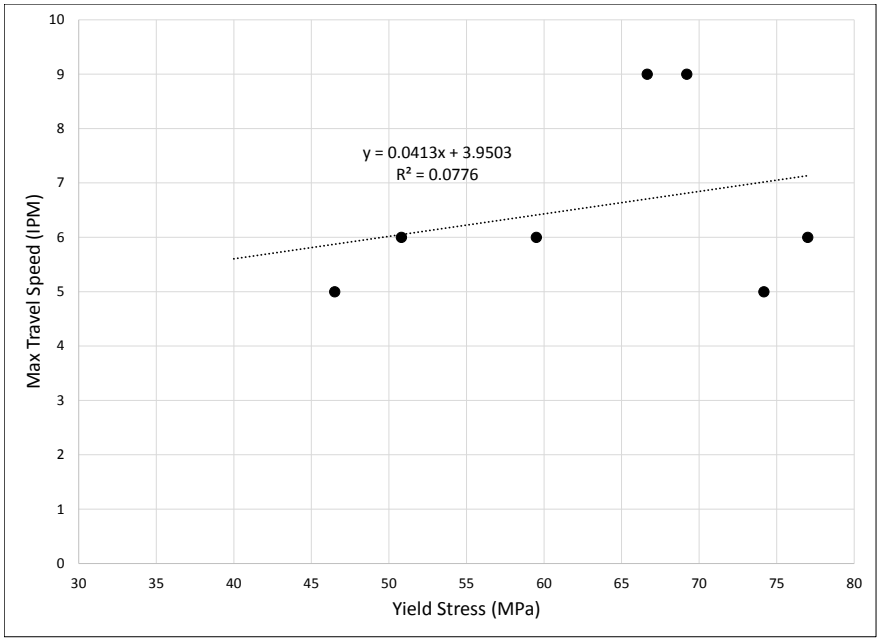

Figure 4.19: A comparison of observed maximum travel speed with observed yield stress for the heats from the experimental study. The observed yield stresses were from a testing temperature of 1000 °C.

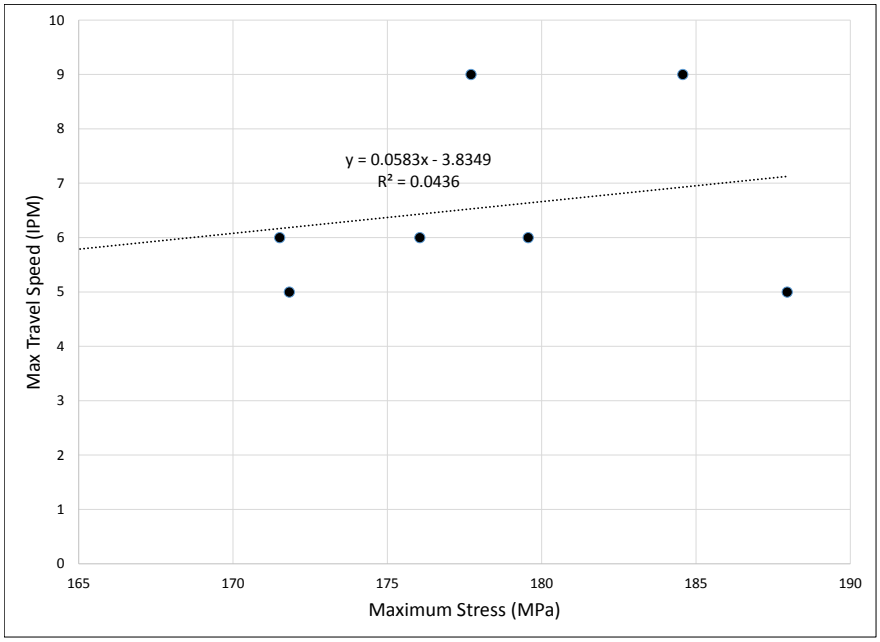

Figure 4.20: A comparison of observed maximum travel speed with observed maximum stress for the heats from the experimental study. The observed maximum stresses were from a testing temperature of 1000 °C.

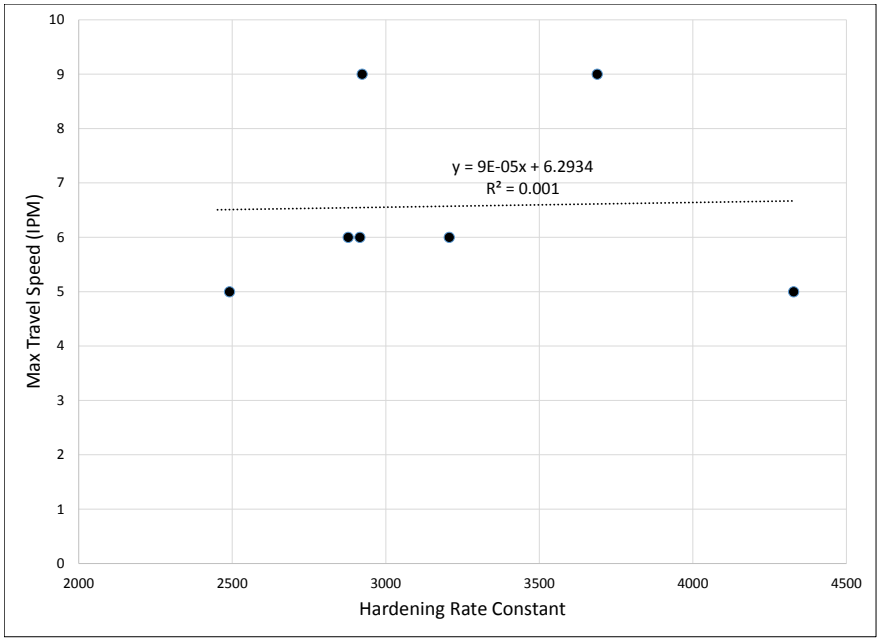

Figure 4.21: A comparison of observed maximum travel speed with observed hardening rate constant for the heats from the experimental study. The observed hardening rate constant were from a testing temperature of 1000 °C.

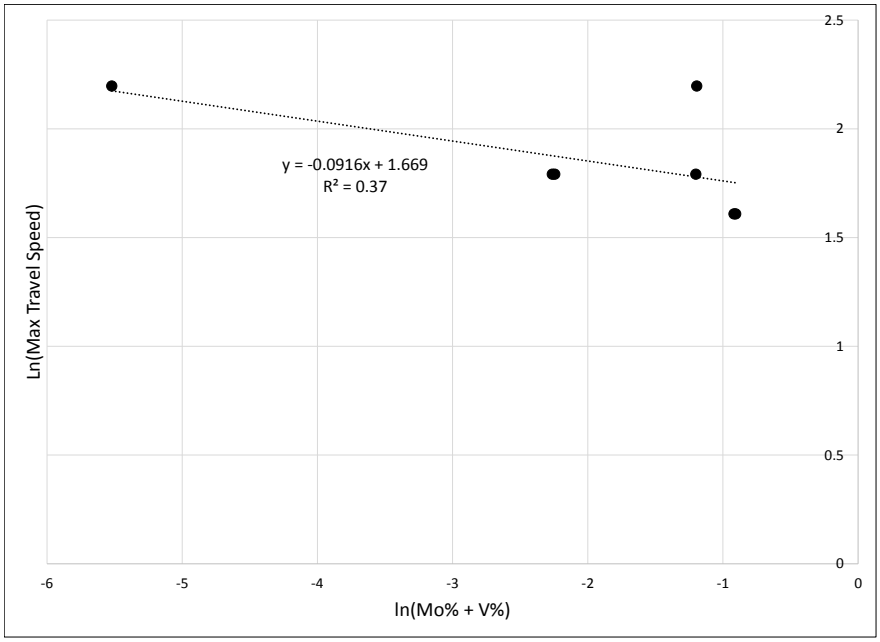

Figure 4.22: A log-log plot of both max travel speed and %Mo + %V content for each heat. The appearance of 5 data points as opposed to the expected 7 is due to several of the heats having the same molybdenum and vanadium content and friction stir weldability.

None of the relationships presented in these figures show substantial correlation. The R^2 values for friction stir weldability correlating with yield stress, maximum stress, and hardening rate constant are 0.0776, 0.0436, and 0.001, respectively. These values indicate that the variables are not related. The R^2 value between the natural log of friction stir weldability and the natural log of molybdenum and vanadium content is much better, at 0.37, but far worse than the R^2 value of 0.9982 found for the same relationship in the preliminary heats.

These unexpected results led to further analysis of the welds that were used to obtain each heat's friction stir weldability. This analysis was done to determine if conclusions drawn from the experimental heats' friction stir weldability are valid, or if there were problems in the experiments used to obtain the friction stir weldability data. This analysis is found in Section 4.7.

4.6 Welding Force Analysis

The friction stir welding machine utilized to create the welds recorded data from each weld, including travel speed, forces in the x, y, and z directions, and spindle torque. This data was recorded several times a second, and a record was created for analysis.

These welds were composed of four sections along the length of the weld, each characterized by a different travel speed. The first section was used to ramp the travel speed up from 0 ipm to the first welding speed, followed by three segments run at the three travel speeds being tested in that weld. A record of which travel speeds were tried in each weld, along with the tool temperature reached at each weld segment, can be found in Appendix F.

The forces looked at were the x-force (along the axis of travel), the z force (the force exerted downward by the pin tool into the plate), and the spindle torque (the force required to spin the pin tool in the material). Force in the y direction (perpendicular to and in plane with the x direction) was negligible, as no movement was required in that axis.

When examining the welding force data, it was discovered that at each change of travel speed, the welding forces would spike, and then taper off to the force level for that travel speed. A graph of x force versus position of a characteristic weld is shown is Figure 4.23, showing the peak values at each travel speed change, which then settles into an average force value. These peaks are primarily caused by the system slightly overshooting the new force as it attempts to come into equilibrium. Because the peak value was noticeably higher in the graphs of certain welds, it was

decided to record both the peak and an average value for each welding force at that travel speed for analysis. A complete listing of these values for all welds can be found in Appendix E.

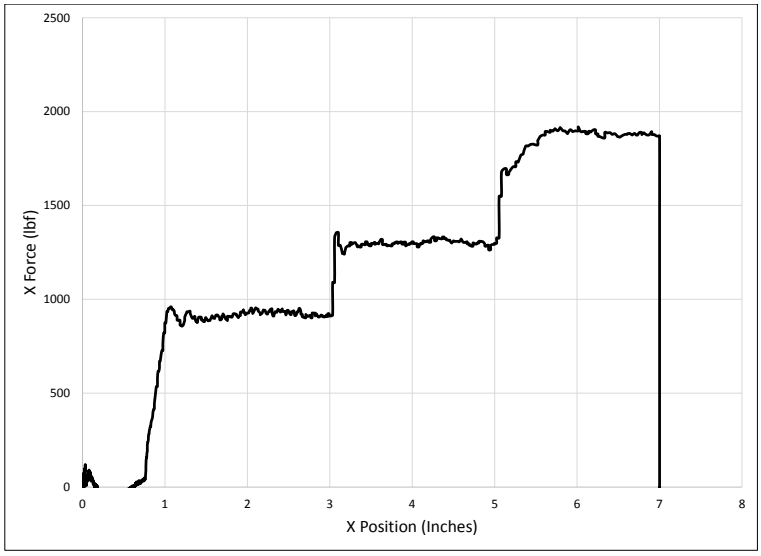

Figure 4.23: The x force recorded at each position of the weld run in 187 at 5/7/9 ipm.

In order to understand general trends for all welds performed at each travel speed, values of welding force were averaged for all welds run at that travel speed. These values can be seen in Figures 4.24, 4.25, and 4.26. Plots of the weld forces for each individual weld segment can be found at the end of Appendix E shows the spread of values across the heats.

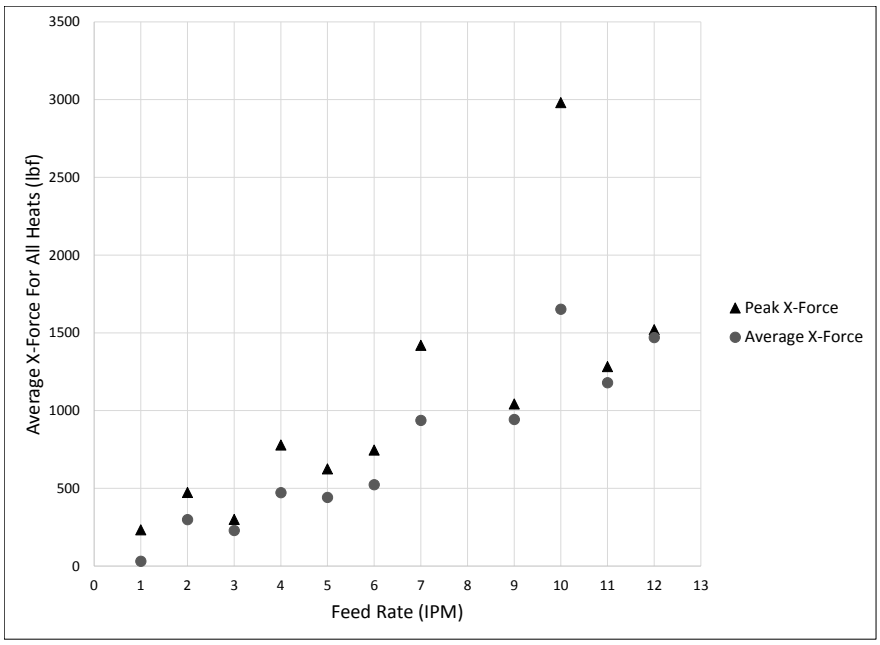

Figure 4.24: The peak and average welding force in the X direction (along the axis of travel) for each heat. The values for all heats run at that travel speed have been averaged together.

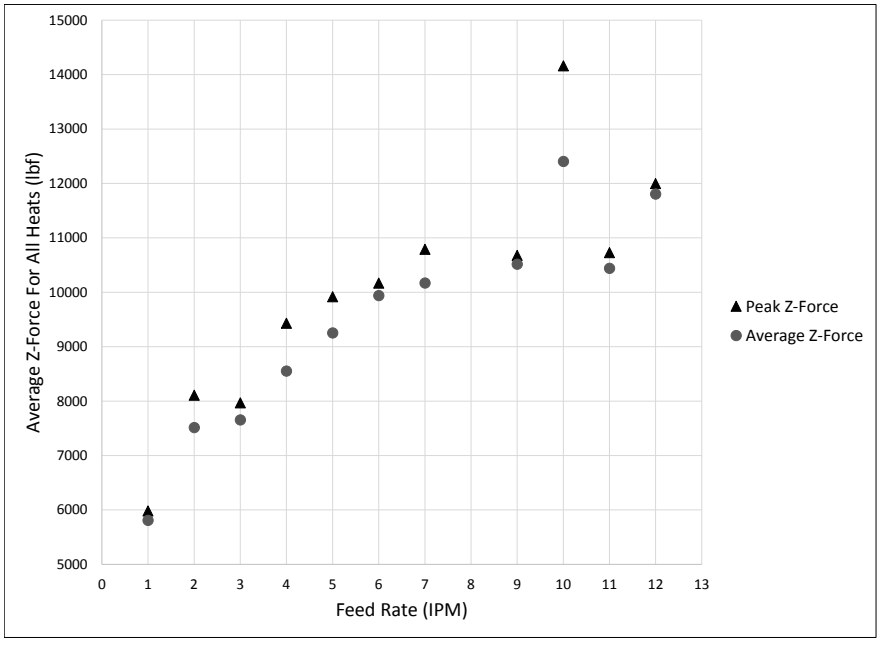

Figure 4.25: The peak and average welding force in the Z direction (into the plate from the top) for each heat. The values for all heats run at that travel speed have been averaged together.

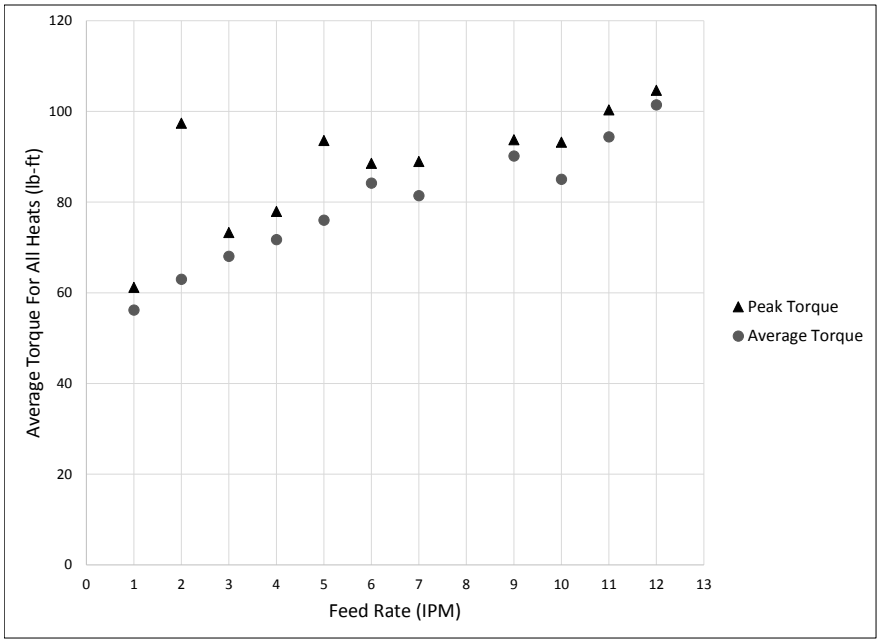

Figure 4.26: The peak and average torque exerted by the tool for each heat. The values for all heats run at that travel speed have been averaged together.

All three welding forces showed a positive relationship with travel speed, as was expected. At increasing travel speeds, more force should be required to move the tool through the material, as the material has not had as long to soften before the tool gets to it.

At most travel speeds, the peak values of x and z force lie close to the averaged value, except for at travel speeds of 7 and 10 ipm. The reasons for this are analyzed more fully in Section 4.7.

Weld Forces and High Temperature Properties

To better understand the role high temperature properties play in friction stir welding, the relationship between the weld forces experienced and the high temperature properties of each heat was examined. Because each heat experienced different weld forces at each travel speed, it was necessary, when comparing weld force to high temperature properties, to use weld forces recorded at the same travel speed. Due to insufficient welding material, no one travel speed included welds run from all eight experimental heats. Travel speeds of 4 and 6 IPM were tested in all experimental steels, and so those travel speeds were chosen for comparing weld forces to high temperature

properties. In both 4 and 6 IPM, weld force data for heat 187 could not be recovered, and so is not used in this analysis.

Graphs of the relationships of the x force, z force, and torque of the welds to their high temperature yield stress, maximum stress, and hardening rate constant are shown in Figures 4.27 to 4.35. Each graph shows the relationships seen at 4 IPM and 6 IPM. In all cases, the relationship between the weld force and the high temperature property is more pronounced at the lower travel speed. It is uncertain what causes this interaction, and whether this interaction with travel speed would be seen with increasing travel speeds. Additional research, outside the scope of this paper, would be required to understand this interaction. Quadratic relationships were found to be appropriate in some cases, as described below, and so are shown in the figures.

The relationships between high temperature properties and weld forces were examined both graphically and by analysis of variance with an alpha threshold of 0.05 [26]. Many data points are scattered far from the line of regression, indicating a high likelihood of outliers. To influence of these outliers, Cook's distance analysis [24] was also performed on each data set.

The p-values from the analysis of variance test for all combinations at 4 and 6 IPM are shown in Tables 4.5 and 4.6.

Table 4.5: The p-values for the relationships between high temperature properties and weld forces for welds run at 4 IPM. P-values highlighted in gray are statistically significant.

	X Force	Z Force	Torque
Yield Stress	0.0310	0.0259	0.2439
Maximum Stress	0.0282	0.1999	0.2001
Hardening Rate Constant	0.0026	0.2149	0.1691

Table 4.6: The p-values for the relationships between high temperature properties and weld forces for welds run at 6 IPM. P-values highlighted in gray are statistically significant.

	X Force	Z Force	Torque
Yield Stress	0.0670	0.1442	0.6133
Maximum Stress	0.1186	0.4861	0.6771
Hardening Rate Constant	0.0343	0.2531	0.3796

According to the analysis of variance, at 4 IPM four relationships are significant: x force with all high temperature properties, and z force with yield stress. At 6 IPM, only one relationship is significant: x force with hardening rate constant.

Cooks distance analysis of these five relationships show that x force as a function of yield stress, x force as a function of maximum stress, and z force as a function of yield stress are all dominated by significant outliers. These outliers, along with the low number of data points, lead us to suspect that these linear correlations do not represent physical relationships between the properties in question.

Further analysis of the residuals of these linear regression lines revealed a quadratic relationship in the cases of x force as a function of yield stress, x force as a function of maximum stress, and z force as a function of yield stress. These quadratic relationships can be seen in Figures 4.27, 4.28, and 4.30. The reasons for this apparent dip in welding force at intermediate stress levels are unknown, but exploration of them could provide insight into the lack of correlation found in the other relationships explored in this section. Such exploration is outside the scope of this paper, but would be potentially useful.

The only linear relationship that is significant and not dominated by outliers is x force and hardening rate constant, at both 4 and 6 IPM. Because this relationship was found at both travel speeds, was found statistically significant, and was not dominated by outliers, it is likely that there is an actual relationship between the hardening rate constant of a HSLA steel, and the x-force experienced in a friction stir weld made in that steel.

This relationship indicates that materials that experience a higher strain hardening rate at the welding temperature require more force to move the tool in the traverse (x) direction. This result makes sense when examined. A material that strain hardens more quickly under welding conditions will more strongly resist forward movement of the tool. More testing is required to analyze the extent of this relationship, and the effect it might have on friction stir welding of HSLA steels.

4.6.1 Weld Forces and Friction Stir Weldability

Because weld forces showed a good relationship with travel speed, it was decided to explore the relationship between weld forces and friction stir weldability in the experimental heats.

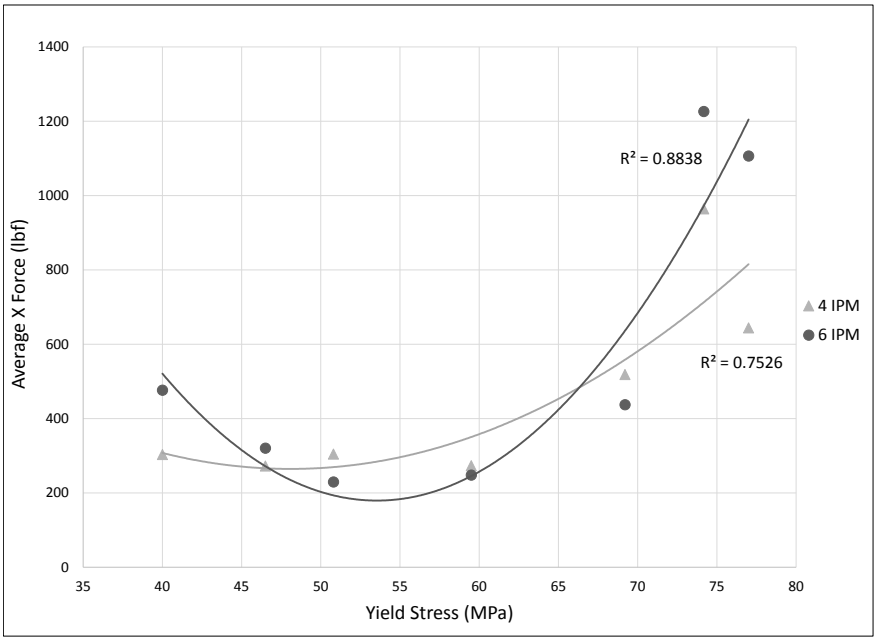

Figure 4.27: The average x force as a quadratic function of the yield stress for heats run at 4 and 6 ipm.

Figures 4.36 to 4.38 show the relationships between weld forces at 4 and 6 ipm with the friction stir weldability of the heats being welded. Values from heats 187 and 185 were not used do to insufficient data. No weld force data at 4 and 6 ipm is available for heat 187, and no friction stir weldability value was determined for heat 185.

No relationship between weld forces and friction stir weldability can be observed in the heats examined, based on our data.

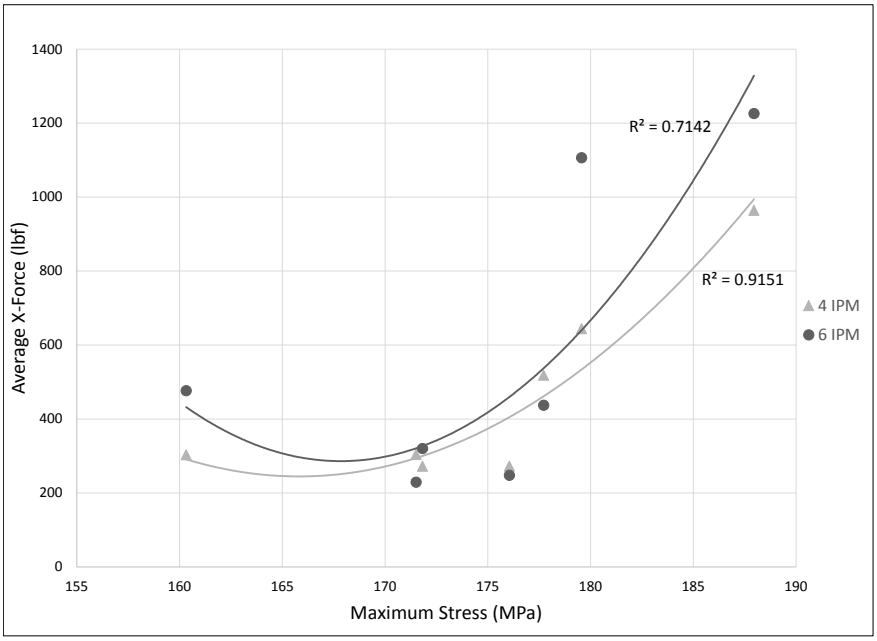

Figure 4.28: The average x force as a quadratic function of the maximum stress for heats run at 4 and 6 ipm.

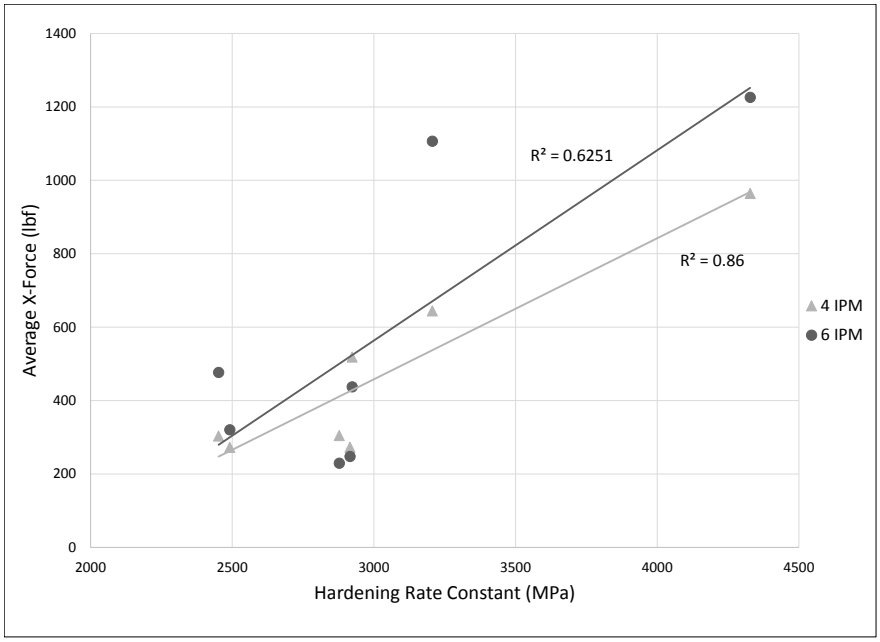

Figure 4.29: The average x force as a function of the hardening rate constant for heats run at 4 and 6 ipm.

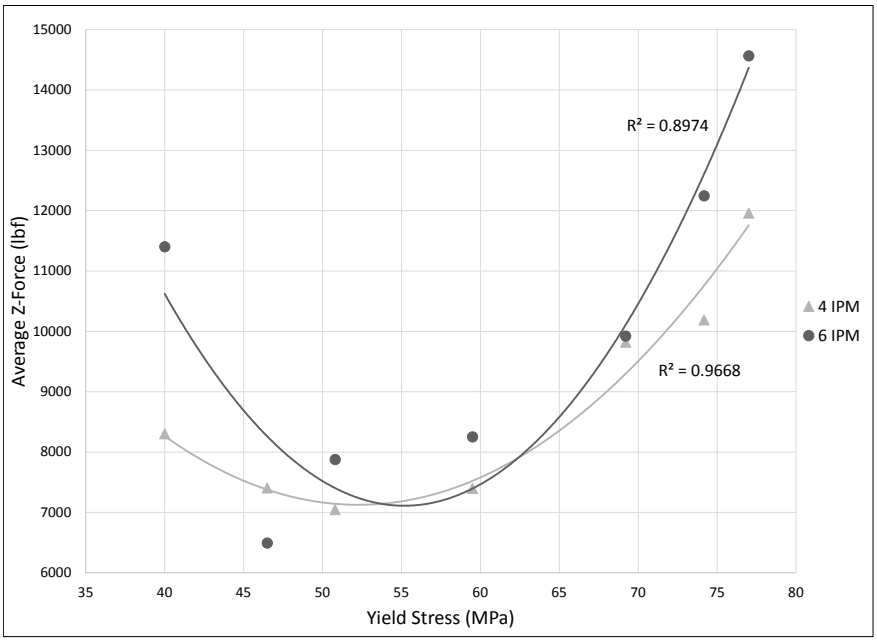

Figure 4.30: The average z force as a quadratic function of the yield stress for heats run at 4 and 6 ipm.

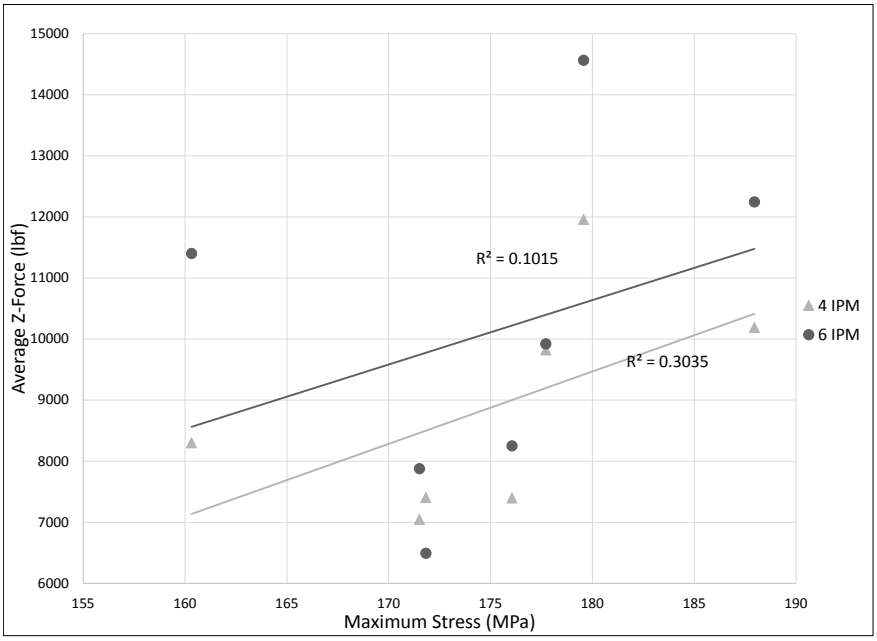

Figure 4.31: The average z force as a function of the maximum stress for heats run at 4 and 6 ipm.

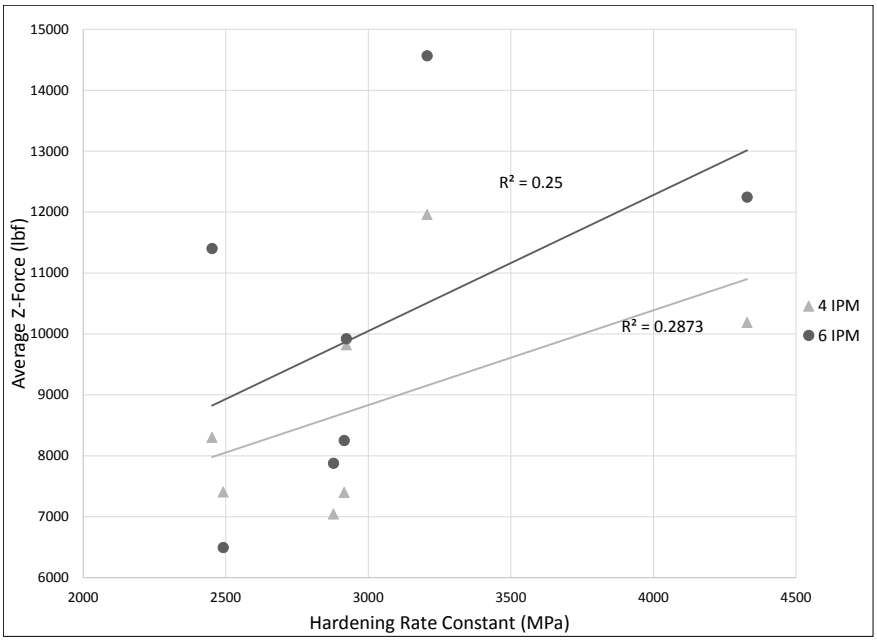

Figure 4.32: The average z force as a function of the hardening rate constant for heats run at 4 and 6 ipm.

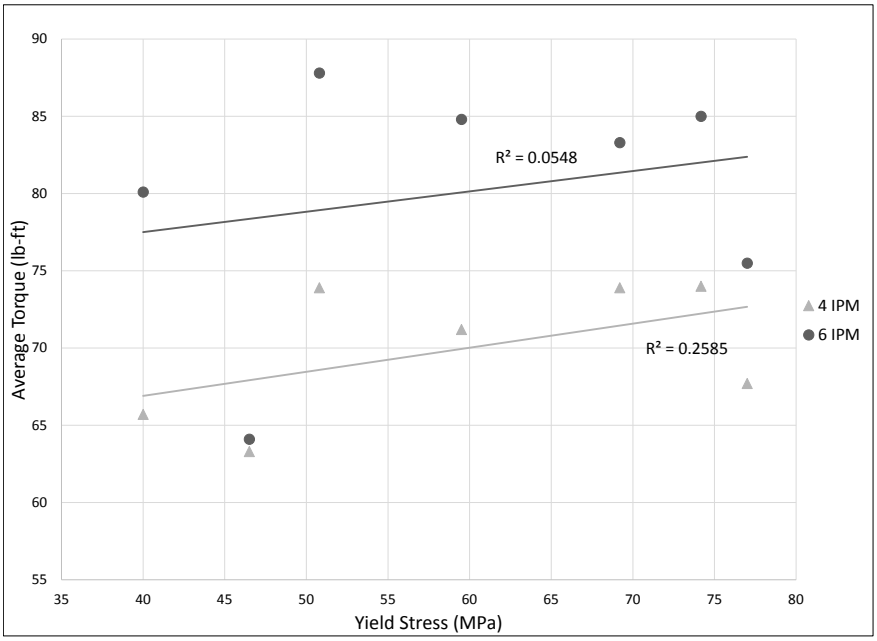

Figure 4.33: The average torque as a function of the yield stress for heats run at 4 and 6 ipm.

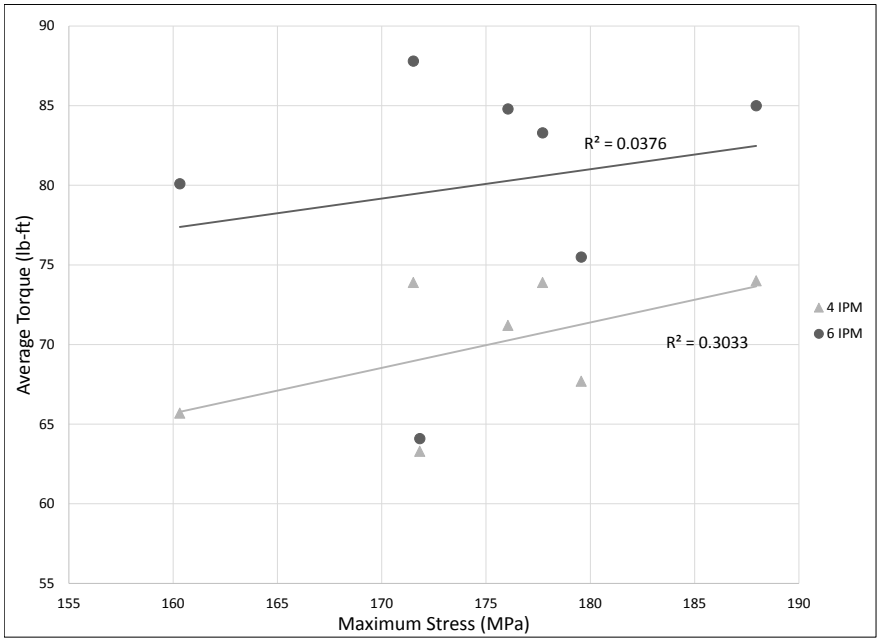

Figure 4.34: The average torque as a function of the maximum stress for heats run at 4 and 6 ipm.

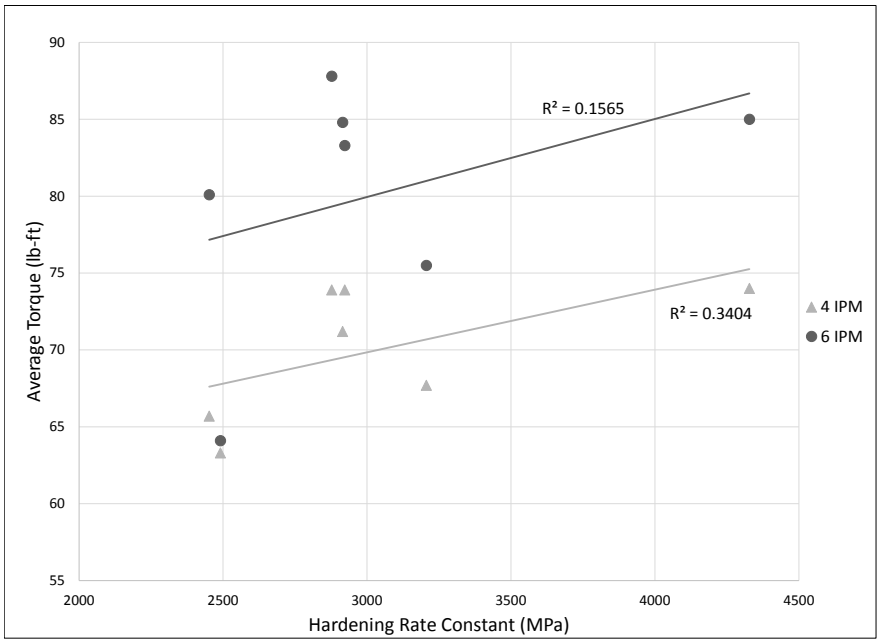

Figure 4.35: The average torque as a function of the hardening rate constant for heats run at 4 and 6 ipm.

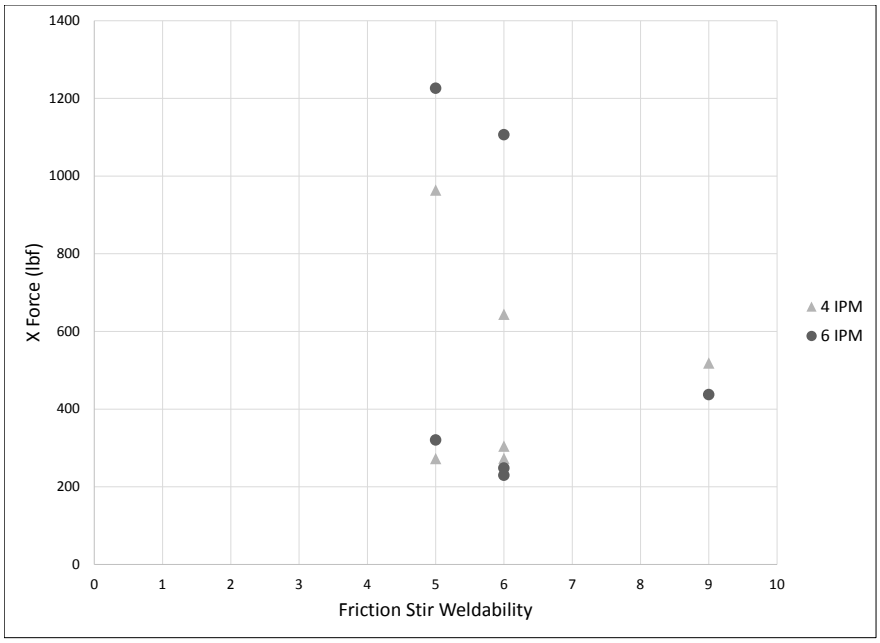

Figure 4.36: The x force experienced at 4 and 6 ipm versus the friction stir weldability of the heats being welded.

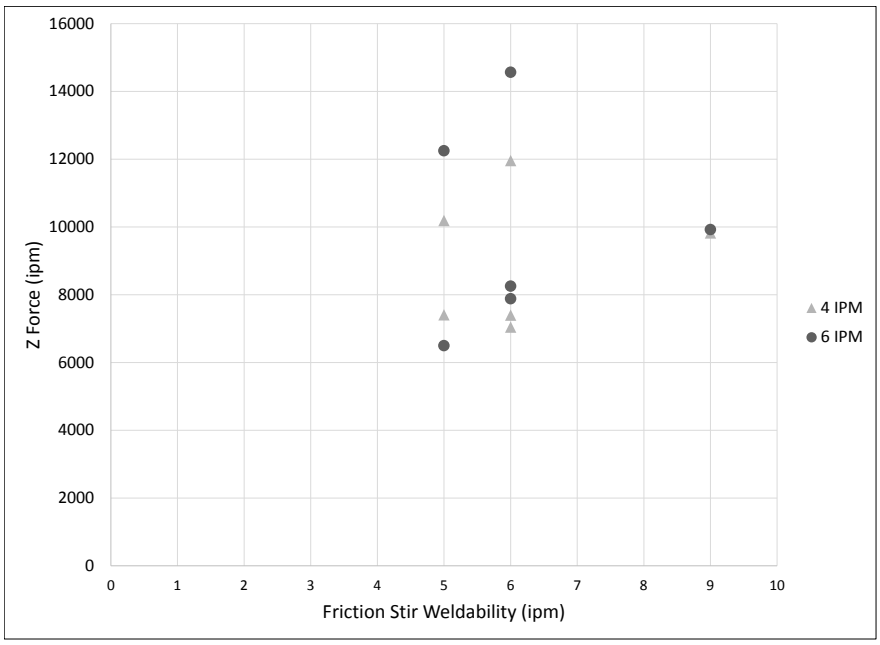

Figure 4.37: The z force experienced at 4 and 6 ipm versus the friction stir weldability of the heats being welded.

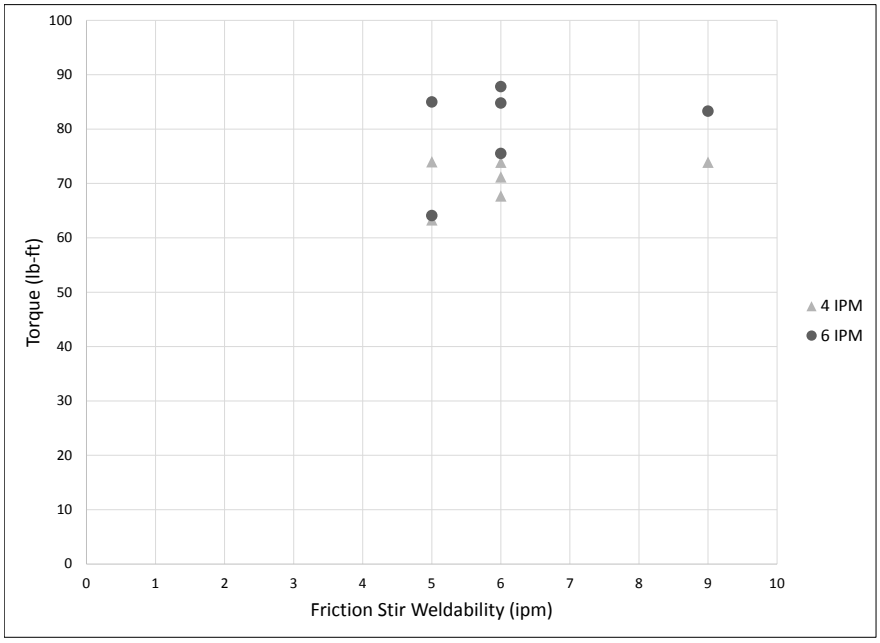

Figure 4.38: The torque experienced at 4 and 6 ipm versus the friction stir weldability of the heats being welded.

4.7 Weld Quality Analysis

As discussed at the beginning of Section 4.4, due to insufficient material, the process used during the preliminary study to determine friction stir weldability was not able to be used with the experimental heats. The size of the plates available also required much shorter welds than were used in the preliminary study, leading to more aggressive ramp up sections of weld. These changes make it difficult to compare friction stir weldability data between the preliminary study alloys and the experimental heats. There is also a lack of friction stir weldability data for heat 185, caused by insufficient welding material of that heat.

Examining the weld force data also revealed areas of concern in need of further analysis. When the weld transitioned from one travel speed segment to the next, the weld force would spike to a peak value before leveling off to an average force value for that segment. The average and peak values for most forces and feed rates were relatively close together. However, examination of the x force chart revealed anomalies at feed rates of 7 ipm and 10 ipm, in which the peak force is significantly greater than the average force for those feed rates.

Looking at the individual welds run at those travel speeds, it was noticed that several welds experienced a significant peak jump in x force at the end of the ramp up period leading into the first welding travel speed. An example of this significant peak can be seen in Figure 4.39. This peak can be compared with the normal x-force peaks, as shown in Figure 4.23.

Examinations of the individual weld force data show that all welds with initial weld speeds of 7 or 10 ipm exhibit this same high peak. These were the fastest initial weld speeds attempted, with correspondingly shorter ramp up times. Each of these welds experienced a massive x force spike at the end of the ramp up section of the weld, when the weld transitioned into the initial testing speed. Coincident with this x force spike, a loud, audible bang was heard from each weld. Based on this information, and the difficulty experienced in clamping the plates due to their small size, it is assumed that the plates experienced a shift in their x location at the end of the ramp up section of travel speed. Markings on the backing plate (consistent with a plate slip), corroborate this theory. The ramp up times experienced by the other welds were gradual enough to avoid this shift. At the x location of the peak x force, a noticeable defect can be observed on the surface of each weld affected by this peak. It is possible that the defects observed in these higher travel speed

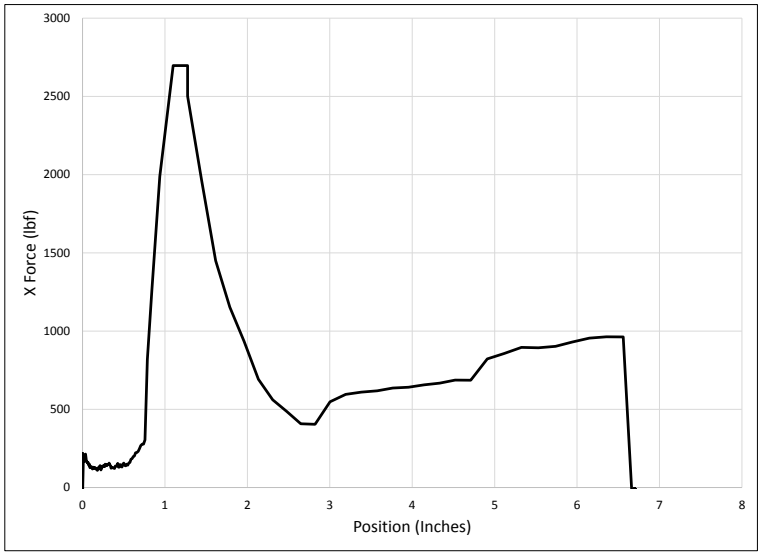

Figure 4.39: The x force recorded at each position of the weld run in 187 at 10/11/12 ipm.

welds were caused by the abrupt shift the plate experienced, and not by the inherent friction stir weldability of each plate.

Appendix G shows the travels speeds run during each weld, and whether a plate slip occurred during that weld.

Heats affected by the plate slipping are: 182, 184, 186, 187, and 188. Because of a lack of material, no friction stir weldability value was found for heat 185. Friction stir weldability values uncompromised by plate slipping were found in heats 183 and 186, but the full process window was not examined to determine if they are the actual friction stir weldability values for these heats. In light of these issues, the friction stir weldability values determined for the experimental heats should be considered the lower bounds for friction stir weldability for these heats. Their friction stir weldability is at least that high, but might be greater.

The friction stir weldability lower bound data that we have allows for initial examinations of the relationships explored in Sections 4.5 and 4.6.1, as presented in those sections. Additional material and welds would be needed to determine the actual friction stir weldability values for the experimental heats if these relationships in the experimental heats were wished to be explored further.

This additional research is unnecessary for the purposes of this study. The quality of the friction stir weldability data for the preliminary study steels, coupled with the quality of our high temperature predictive equations, has allowed us to adequately determine that there is no relationship between high temperature physical properties and friction stir weldability in HSLA steels.

CHAPTER 5. CONCLUSIONS

By performing high temperature compression tests on experimental heats of HSLA steel, using a Gleeble 3500 system, and analyzing the data obtained from the tests, we developed linear models (Equations 4.12, 4.13, and 4.14) to predict high temperature yield stress, maximum stress, and hardening rate constants as a function of chemical composition and testing temperature. These equations were corroborated by comparison between our maximum stress model and a maximum stress model developed by Medina et al. [23]. Conclusions drawn from these models include:

1. For high temperature yield stress, titanium and niobium content were found to be most influential, with increasing percent alloying weight having a positive correlation. Molybdenum was found to have a small positive effect, and yield stress was found to fall with increased temperature, as expected. Vanadium had no effect on yield stress.

2. For high temperature maximum stress, titanium and niobium again were found to be most influential, with both molybdenum and vanadium having small effects. All four alloying elements had a positive relationship with maximum stress. Increasing temperature caused a decrease in maximum stress, as expected.

3. For high temperature hardening rate constant, niobium was found to be most influential, with titanium and vanadium also having large influences. All three had a positive influence on the hardening rate constant. Molybdenum was found to have a negative relationship with hardening rate constant, as was temperature.

4. These equations allow estimation of high temperature physical properties for HSLA steels in the chemical and temperature ranges examined. They have application outside this study, and are one of the principal contributions of this thesis. While the Medina model can be used to estimate peak stress, our models also allow yield stress and the hardening rate constant to be estimated.

These equations allowed us to estimate the high temperature properties for the HSLA alloys used in the preliminary study (Section 2.4). Using these estimated properties, and the friction stir weldability values for each alloy, correlations were calculated between high temperature properties and friction stir weldability for HSLA steels.

Correlations with friction stir weldability were calculated with high temperature yield stress, maximum stress, and hardening rate constant. No relationship exists between the high temperature properties examined and friction stir weldability.

The friction stir weldability of the experimental heats was studied, but insufficient material was present to obtain adequate friction stir welding data for definite analysis. Initial analysis of present friction stir weldability data supports correlations reached with the preliminary study's data, but was inconclusive.

Considering these results, our original hypothesis, that the high temperature properties of HSLA steels are linked to their friction stir weldability, is disproved. In analysis of the friction stir weldability data, molybdenum and vanadium concentrations showed the highest level of correlation with friction stir weldability. Friction stir weldability of HSLA steels appears linked to composition, but not to high temperature properties as previously thought.

5.1 Future Work

1. The compositional and temperature ranges for which the linear models can accurately predict the high temperature properties of HSLA steels should be examined. This can be accomplished by obtaining additional heats of HSLA steel with compositional ranges outside the ranges examined in this study, performing Gleeble compression tests on them, and comparing the empirically determined high temperature physical properties with those predicted by the linear models. Gleeble compression tests should also be performed at temperatures outside our testing range, for the same reason.

2. The two factor confounded interactions in the linear models should be unconfounded by creating an additional 8 heats of HSLA steel according to a fold-over statistical design of experiments. This would clarify which interaction terms are important in our linear equations.

3. Additional, longer plates of our 8 experimental heats should be obtained, and their friction stir weldability should be accurately determined, using the same procedure used in the preliminary study (see Section 2.4). This procedure varies both travel speed and spindle speed to examine an entire parameter window to find the friction stir weldability for a heat. This would allow more accurate analysis of the effect of micro-alloying composition on friction stir weldability in HSLA steels.

REFERENCES

[1] Fletcher, E., 1979. *High-strength, low-alloy steels: status, selection, and physical metallurgy*. Battelle Press, Columbus, Oh. 1, 4

[2] Sorensen, C., and Nelson, T., 2010. Development of a friction stir weldability index for hsla alloys in CFSP Presentation at Brigham Young University: Provo, Ut. 1, 5

[3] Sampath, K., 2006. "An understanding of hsla-65 plate steels." *Journal of Materials Engineering and Performance,* **15**, pp. p. 32–40. 3, 4

[4] Davis, J., 1996. Carbon and alloy steels. 3, 4

[5] ASM, 1990. High-strength structural and high-strength low-alloy steels. 3, 4

[6] Corporation, U. S. S., and McGannon, H., 1971. *The making, shaping and treating of steels*., 9th ed. United State Steel, Pittsburgh, Pa. 4

[7] DeGarmo, E., 2008. *Materials and Processes in Manufacturing*. Wiley, Hoboken, N.J. 4

[8] Maalekian, M., 2011. "Solid-state transformations in weldments." In *Welding Fundamentals and Processes, Vol 6A, ASM Handbook*. ASM, pp. p. 122–145. 4, 5

[9] Tsai, C., 2011. "Heat flow in fusion welding." In *Welding Fundamentals and Processes, Vol 6A, ASM Handbook*. ASM International, pp. p. 55–66. 5

[10] Shome, M., and Mohanty, O., 2006. "Continuous cooling transformation diagrams applicable to the heat-affected zone of hsla-80 and hsla-100 steels." *Metallurgical and Materials Transactions A,* **37**(7), pp. p. 2159–2169. 5

[11] Shome, M., 2007. "Effect of heat-input on austenite grain size in the heat-affected zone of hsla-100 steel." *Materials Science and Engineering: A,* **445-446**, pp. p. 445–460. 5

[12] Thomas, W., and et al, 1991. Friction-stir butt welding, Dec. 5

[13] Nandan, R., DebRoy, T., and Bhadeshia, H., 2008. "Recent advances in friction-stir welding process, weldment structure and properties." *Progress in Materials Science,* **53**(6), pp. p. 980 – 1023. 5

[14] Thomas, W., Thredgill, P., and Nicholas, E., 1991. "Feasibilty of friction stir welding steel." *Science and Technology of Welding & Joining,* **4**, pp. p. 365–372. 5

[15] Lohwasser, D., and Chen, Z., eds., 2010. *Friction Stir Welding: From Basics to Applications*. CRC Press. 5

[16] Sorensen, C., and Nelson, T., 2007. "Friction stir welding of ferrous and nickel alloys." In *Friction stir welding and processing*, R. Mishra and M. Mahoney, eds. ASM International, Materials Park, Ohio, pp. p 111–122. 5

[17] Evans, R., and Scharning, P., 2011. "Axisymmetric compression test and hot working properties of alloys." *Material Science Technology,* **Vol 17**, pp. p192–197. 14

[18] Kuhn, H., 2000. "Uniaxial compression testest, mechanical testing and evaluation." *ASM Handbook,* **Vol 8**, pp. p 143–151. 15

[19] Dieter, G., 2000. "Mechanical behavior under tensile and compressive loads." *Mechancial Testing and Evaluation, Vol 8, ASM Handbook*, pp. p. 99–108. 16, 17

[20] Kocks, U. F., and Mecking, H., 2003. "Physics and phenomenolgy of strain hardening: the fcc case." *Progress in Ma,* **Vol 48**, pp. p 171–273. 18

[21] Chartrand, R., 2011. "Numerical differentiation of noisy, nonsmooth data." *International Scholarly Reserach Network: Applied Mathematics*. 18

[22] Navidi, W., 2011. *Statistics for Engineers and Scientists 3rd Edition*. McGraw Hill. 23

[23] Medina, S. F., and Hernandez, C. A., 1996. "General expression of the zener-hollomon parameter as a function of the chemical composition of low alloy and microalloyed steels." *Acta mater,* **44**, pp. p 137–148. 26, 27, 53

[24] Cook, R. D., 1977. "Detection of influential observation in linear regression." *Technometrics,* **Vol. 19**, pp. p. 15–18. 28, 41

[25] Cook, R. D., and Weisberg, S., 1982. *Residuals and Influence in Regression*. Chapman & Hall. 28

[26] Field "Analysis of variance." *Encyclopedia of measurement and statistics*, pp. p 33–36. 41

APPENDIX A. STEEL TOOL DRAWING

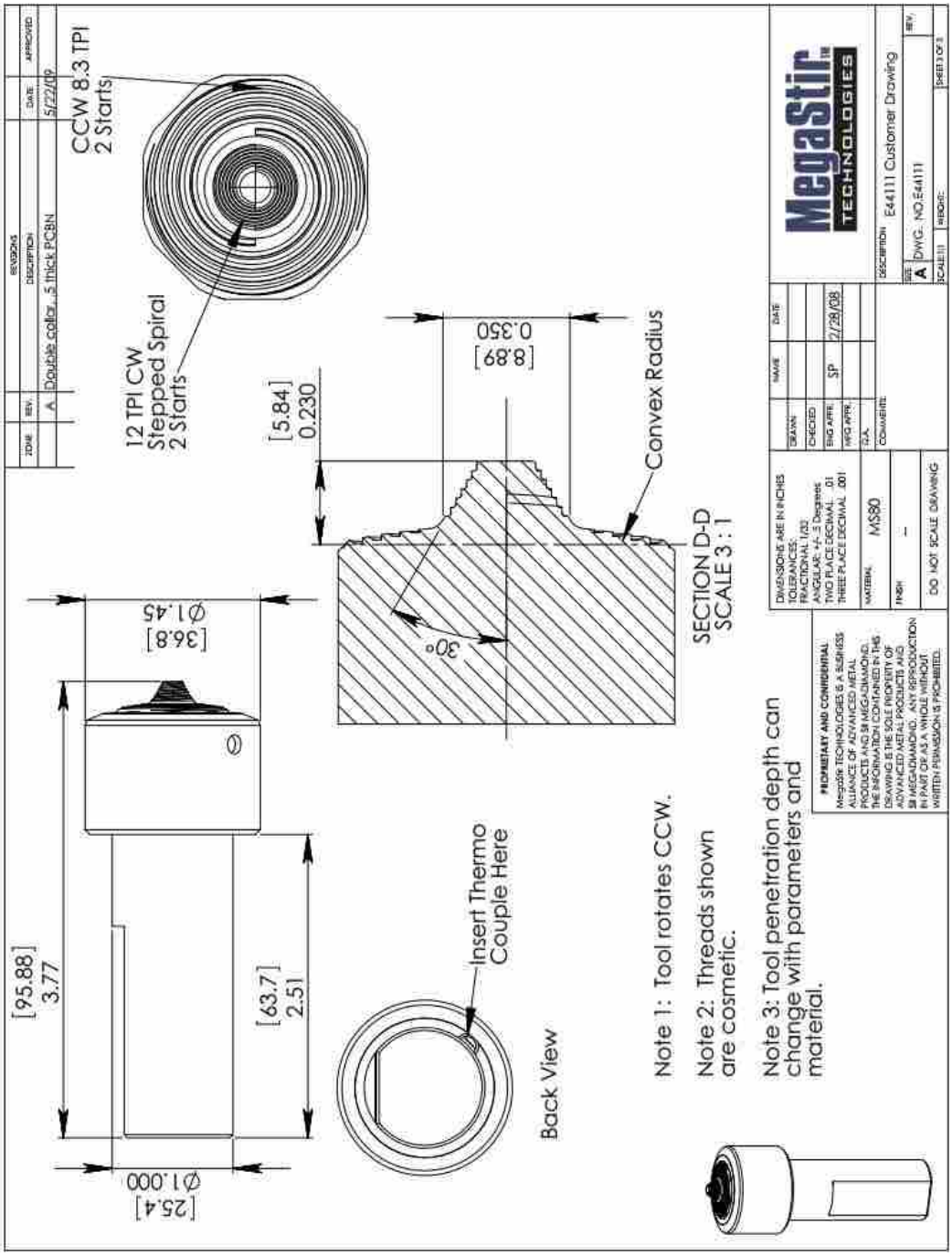

Figure A.1: Figure **??** - PCBN CS4 tool: Model E44111

APPENDIX B. GLEEBLE SAMPLE MEASUREMENTS

Table B.1: Physical measurements of the samples used in the gleeble compression tests. $\mathbf{D_o}$ and $\mathbf{H_o}$ represent the average starting diameter and height of the samples for that heat. Each sample's diameter was measured at the top, and at the maximum diameter along the bulge. Each diameter was measured twice to account for ovality. The top diameter measurements are recorded as $\mathbf{D_{t1}}$ and $\mathbf{D_{t2}}$, and the bulge diameter measurements are recorded as $\mathbf{D_{b1}}$ and $\mathbf{D_{b2}}$. The crushed height is recorded as $\mathbf{H_c}$.

Sample	D_o	H_o	D_{t1}	D_{t2}	D_{b1}	D_{b2}	H_c	Barreling (%)	Ovality (%)
182-950 C	12.1793	12.22	14.06	14.15	14.64	14.65	8.7	2.94	0.64
182-1000 C	12.1793	12.22	13.96	13.93	14.87	14.78	8.7	5.49	0.22
182-1100 C	12.1793	12.22	14.09	14.14	14.75	14.8	8.62	3.81	0.35
183-950 C	12.1818	12.18	13.91	13.92	14.74	14.71	8.71	4.49	0.07
183-1000 C	12.1818	12.18	14	14.1	14.74	14.8	8.65	4.40	0.71
183-1100 C	12.1818	12.18	13.91	14.09	14.66	14.86	8.59	3.54	1.29
184-950 C	12.1666	12.18	14.1	14.04	14.74	14.76	8.64	4.26	0.42
184-1000 C	12.1666	12.18	14.11	14.12	14.73	14.73	8.68	4.46	0.07
184-1100 C	12.1666	12.18	13.89	13.87	14.96	14.97	8.61	6.95	0.14
185-950 C	12.1742	12.21	14.17	14.14	14.65	14.78	8.7	4.10	0.21
185-1000 C	12.1742	12.21	14.05	14.1	14.73	14.65	8.68	3.51	0.35
185-1100 C	12.1742	12.21	14.14	14.12	14.82	14.76	8.6	3.95	0.14
186-950 C	12.1768	12.21	13.9	13.87	14.67	14.74	8.67	3.55	0.22
186-1000 C	12.1768	12.21	14.25	14.16	14.77	14.65	8.64	3.27	0.63
186-1100 C	12.1768	12.21	14.14	14.14	14.75	14.84	8.62	4.22	0
187-950 C	12.1844	12.17	14	14.01	14.73	14.76	8.75	5.29	0.07
187-1000 C	12.1844	12.17	14.06	14.1	14.72	14.82	8.7	5.05	0.28
187-1100 C	12.1844	12.17	14.1	14.16	14.77	14.85	8.7	5.62	0.42
188-950 C	12.1768	12.19	13.97	14.06	14.72	14.86	8.7	5.29	0.64
188-1000 C	12.1768	12.19	14.13	14.25	14.75	14.74	8.68	4.41	0.84
188-1100 C	12.1768	12.19	14.06	14.13	14.88	14.95	8.57	5.48	0.50
189-950 C	12.179	12.18	14.03	14.08	14.8	14.64	8.74	4.82	0.36
189-1000 C	12.179	12.18	14.13	14.11	14.69	14.73	8.77	5.03	0.14
189-1100 C	12.179	12.18	13.8	13.99	14.65	14.91	8.63	4.34	1.37
Average:	12.1774	12.1925	14.04	14.0742	14.747	14.781	8.669	4.51	0.42
Std Dv:	0.0051	0.0175	0.10657	0.09686	0.0771	0.0909	0.052	0.908	0.361

APPENDIX C. LINEAR MODEL RESIDUALS

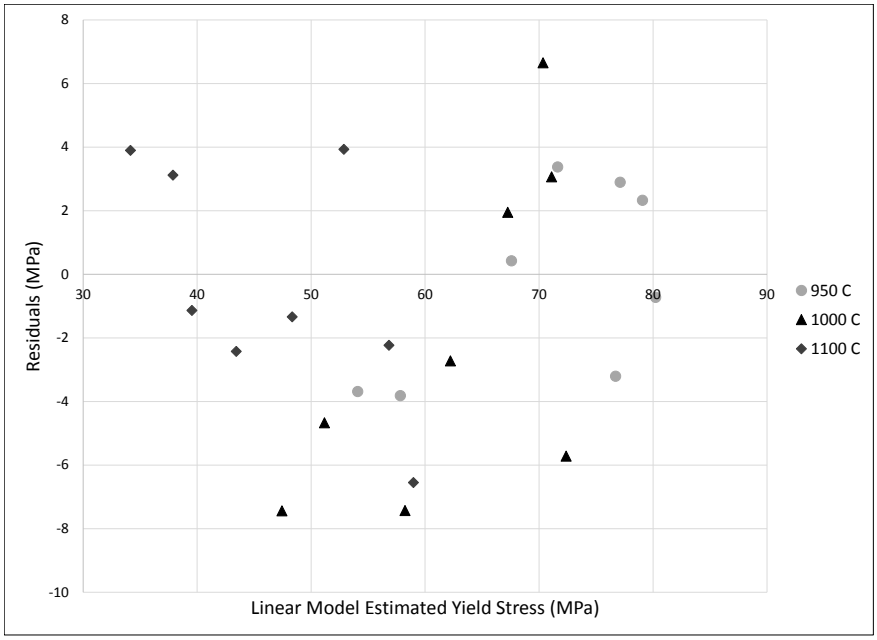

Figure C.1: Residuals plot for the yield stress model showing a good random distribution.

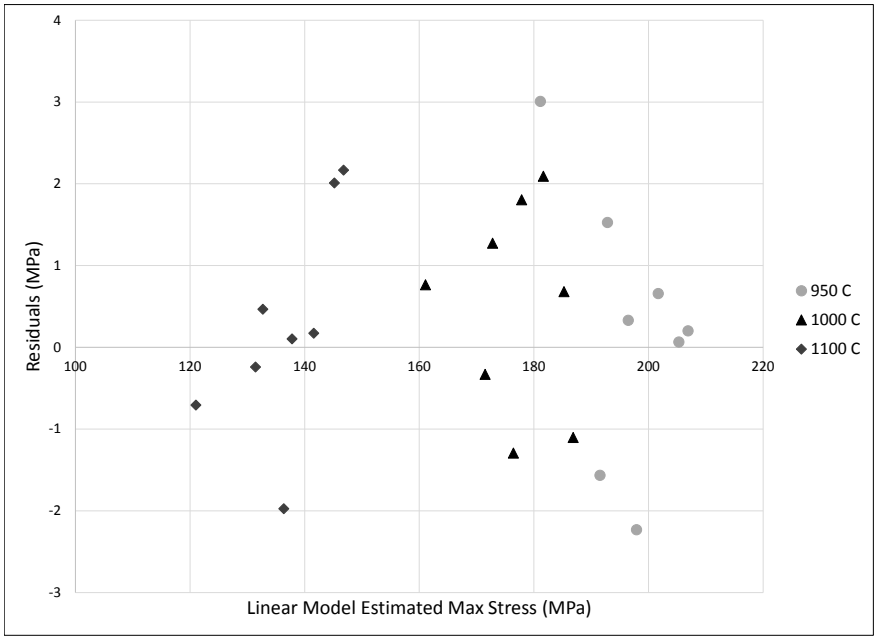

Figure C.2: Residuals plot for the maximum stress model showing a good random distribution.

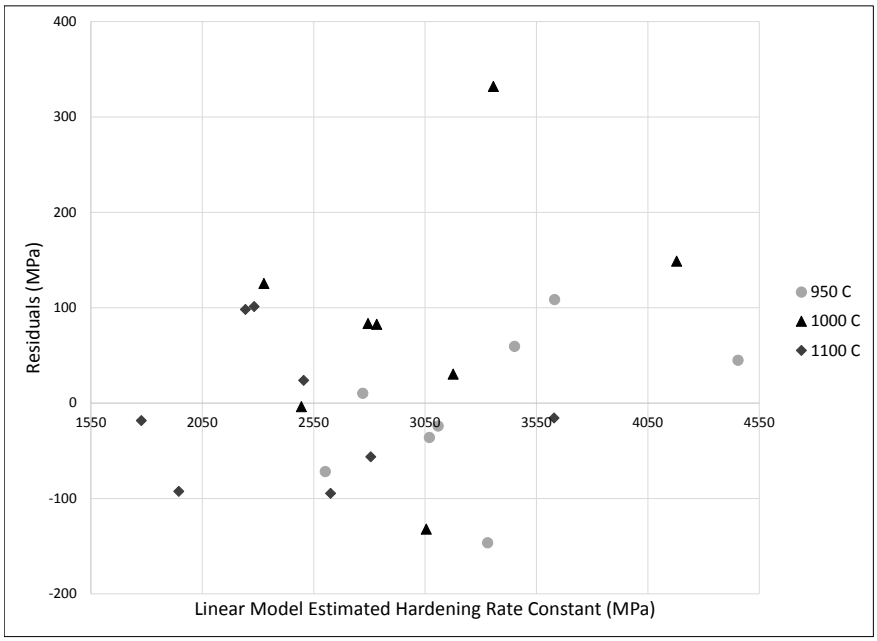

Figure C.3: Residuals plot for the hardening rate model showing a good random distribution.

APPENDIX D. STATISTICAL MODEL

Table D.1: The $2*2^{4-1}$) statistical model used to develop the linear models used to predict yield stress (σ_y), maximum stress (σ_m), and the hardening rate constant (θ_0). The '+' and '-' symbols indicate whether that factor or interaction is held at a high or low value, respectively, for that run in the model. The results for each run are listed on the right. The bottom of the table includes the high and low means ($\overline{Y}_H$ and $\overline{Y}_L$) for the factors and interactions, and their calculated effects and coefficients.

		Factors					Two Factor Interactions							Results		
	Heat	**Temp**	**Mo**	**Nb**	**V**	**Ti**	**Mo*Ti or Nb*V**	**Nb*Ti or Mo*V**	**V*Ti or Mo*Nb**	**Temp*Mo**	**Temp*Nb**	**Temp*V**	**Temp*Ti**	σ_y	σ_m	θ_0
	182	-	-	+	+	-	+	-	-	-	+	+	-	54.6	141.41	2531
	183	+	+	-	+	-	-	+	-	+	-	+	-	41	131.66	1851.9
	184	+	-	+	-	+	-	+	-	-	+	-	+	47	138.32	2528.5
	185	+	-	-	-	-	+	+	+	-	-	-	-	38.05	121.72	1758
	186	+	-	-	+	+	-	-	+	-	-	+	+	38.41	132.25	2342
	187	+	+	+	-	-	-	-	+	+	+	-	-	52.42	143.17	2749.5
	188	+	+	-	-	+	+	-	-	+	-	-	+	41	137.68	2383.8
	189	+	+	+	+	+	+	+	+	+	+	+	+	56.8	144.61	3613.3
	182	-	-	+	+	-	+	-	-	+	-	-	+	80	201.03	3510.4
	183	-	+	-	+	-	-	+	-	-	+	-	+	54	193.09	2780.2
	184	-	-	+	-	+	-	+	-	+	-	+	-	73.5	196.12	3183.7
	185	-	-	-	-	-	+	+	+	+	+	+	+	50.4	178.11	2530
	186	-	-	-	+	+	-	-	+	+	+	-	-	68	191.29	3033.1
	187	-	+	+	-	-	-	-	+	-	-	+	+	81.4	205.22	3739.8
	188	-	+	-	-	+	+	-	-	-	+	+	-	75	200.12	3084
	189	-	+	+	+	+	+	+	+	-	-	-	-	79.5	206.68	44992
σ_y	$\overline{Y}_H$	46.16	60.14	65.65	59.04	1.71	59.42	55.03	58.12	57.89	57.28	58.89	56.13	**Mean**	**Mean**	**Mean**
	$\overline{Y}_L$	70.23	56.25	50.73	57.35	56.48	56.97	61.35	58.26	58.50	59.11	57.50	60.26	58.19	166.405	2882.4
	Effect	-24.07	3.90	14.92	1.69	3.42	2.45	-6.32	-0.14	-0.61	-1.83	1.40	-4.13			
	Coefficient	-12.03	1.95	7.46	0.85	1.71	1.23	-3.16	-0.07	-0.30	-0.92	-0.70	-2.07			
σ_m	$\overline{Y}_H$	136.35	170.28	172.07	167.75	168.38	166.42	163.79	165.38	165.46	166.27	166.19	166.29			
	$\overline{Y}_L$	196.46	162.53	160.74	165.06	164.43	166.39	169.02	167.43	167.35	166.45	166.62	166.52			
	Effect	-60.11	7.75	11.33	2.69	3.96	0.03	-5.23	-2.05	-1.89	-0.28	-0.44	-0.23			
	Coefficient	-30.05	3.87	5.67	1.35	1.98	0.015	-2.62	-1.02	-0.95	-0.14	-0.22	-0.12			
θ_0	$\overline{Y}_H$	2469.75	3087.71	3294.43	3020.14	3083.45	2988.71	2843.10	3033.11	2856.96	2856.20	2859.46	2928.50			
	$\overline{Y}_L$	3295.05	2677.09	2470.38	2744.66	2681.35	2776.09	2921.70	2731.69	2907.84	2908.6	2905.34	2836.3			
	Effect	-825.3	410.63	824.05	275.48	402.10	212.63	-78.60	301.43	-50.88	-52.40	-45.88	92.20			
	Coefficient	-412.65	205.31	412.03	137.74	201.05	106.31	-39.30	150.71	-25.44	-26.20	-22.94	46.10			

APPENDIX E. WELD FORCES

1 IPM

	X Force (lbf)		Z Force (lbf)		Torque (lb-ft)	
Heat	Peak	Average	Peak	Average	Peak	Average
182						
183						
184						
185	184.6	5.2	6023	5844.9	58.5	53.7
186	282.3	57	5940.3	5771.8	63.9	58.7
187						
188						
189						
Average:	233.45	31.1	5981.7	5808.4	61.2	56.2

2 IPM

	X Force (lbf)		Z Force (lbf)		Torque (lb-ft)	
Heat	Peak	Average	Peak	Average	Peak	Average
182	309.6	251.9	9807.8	9209.4	64	57.6
183	175.4	117.7	7041.6	6738.2	59.9	55.7
184	335.5	273.7	8543.6	8098.4	178.6	62.2
185	289.1	102.4	7383.5	6991.5	70.5	59.9
186	305.5	117.4	6648	6377.9	71.1	65.8
187						
188						
189	964.1	704.2	9855.9	8585.2	69.4	64.1
Average:	473.55	299.43	8107.8	7513.3	97.4	63

3 IPM

	X Force (lbf)		Z Force (lbf)		Torque (lb-ft)	
Heat	Peak	Average	Peak	Average	Peak	Average
182						
183						
184						
185	375.7	275.3	8800.3	8324.5	71.6	65.4
186	224.4	182.1	7134.4	6987	75	70.7
187						
188						
189						
Average:	300.05	228.7	7967.4	7655.8	73.3	68.05

4 IPM

	X Force (lbf)		Z Force (lbf)		Torque (lb-ft)	
Heat	Peak	Average	Peak	Average	Peak	Average
182	796.1	644.1	12926	11960	73.2	67.7
183	426.5	272.5	7610	7406.3	67.2	63.3
184	914.1	518.5	10433	9822.8	76.9	73.9
185	387	303.3	9393.6	8302.5	74.2	65.7
186	525.5	304.5	7798.1	7046.2	81.2	73.9
187						
188	376	273	7899.6	7399.1	78.2	71.2
189	1692.6	964.2	11628	10189	79.3	74
Average:	779.04	472.7	9430.5	8551.9	77.96	71.74

5 IPM

	X Force (lbf)		Z Force (lbf)		Torque (lb-ft)	
Heat	Peak	Average	Peak	Average	Peak	Average
182						
183	396.7	165.8	8314.5	7782.9	75.8	68
184	771	288.4	8199.2	7579.8	82.8	73.4
185	483.4	410.8	10869	10370	79	75.1
186	500.4	315.7	8025.4	7945.3	88.8	84.1
187	959.1	917.9	13552	12206	131.9	66.7
188	410	275.2	8948.3	8163.1	85.5	80.8
189						
Average:	624.78	441.6	9918.6	9252.9	93.6	76.02

6 IPM

	X Force (lbf)		Z Force (lbf)		Torque (lb-ft)	
Heat	Peak	Average	Peak	Average	Peak	Average
182	1167.3	1106.7	15265	14566.4	81	75.5
183	466	320.4	7357.8	6494.7	71.7	64.1
184	819.4	437.5	10115	9923.4	86.1	83.3
185	550.1	476.7	11614	11402.7	84.7	80.1
186	393.1	229.5	7988	7879.1	92.6	87.8
187						
188	360.2	248	8437.8	8252.8	89	84.8
189	1609.4	1226.2	12690	12246.9	90.3	85
Average:	746.44	523.58	10169	9940.98	88.54	84.2

7 IPM

	X Force (lbf)		Z Force (lbf)		Torque (lb-ft)	
Heat	Peak	Average	Peak	Average	Peak	Average
182	2310	1727.6	12463	12064	82.5	77
183	496.2	300.7	8136	7939.5	83.2	78.1
184	474.9	224.8	8534.6	8340.6	91.7	86.8
185						
186	1494.1	1134.9	8299.5	7621.3	90.5	77.7
187	1355.1	1294.1	14935	14596	82.6	76.3
188	2353.6	1094.8	11395	10121	91.1	84.9
189						
Average:	1419.4	937.15	10791	10170	88.975	81.425

9 IPM

	X Force (lbf)		Z Force (lbf)		Torque (lb-ft)	
Heat	Peak	Average	Peak	Average	Peak	Average
182	1581.1	1328.9	11336	11014	86.9	84.6
183	567.3	430.6	7979.7	7353.3	85.8	78.4
184	486.8	413.3	8681.3	8543.4	97.4	93.8
185						
186	805.6	743.6		8059.5	92.3	88.6
187	1918.7	1844.8		15322	85.7	81
188	957.8	770	10231	10137	99.6	97.3
189						
Average:	1042.2	942.93	10677	10516	93.75	90.175

10 IPM

	X Force (lbf)		Z Force (lbf)		Torque (lb-ft)	
Heat	Peak	Average	Peak	Average	Peak	Average
182						
183						
184	3264	2169.8	15735	14011	90	86.5
185						
186						
187	2696.9	1135	12586	10801	96.4	83.6
188						
189						
Average:	2980.5	1652.4	14160	12406	93.2	85.05

11 IPM

	X Force (lbf)		Z Force (lbf)		Torque (lb-ft)	
Heat	Peak	Average	Peak	Average	Peak	Average
182	1617.8	1590.7	10433.8	9659.1	86.2	79.3
183						
184	2002.8	1879.2	13513.7	13453	97.7	95.6
185						
186	1278.1	1101.8	8593.1	7652.1	95	78.7
187	686.9	636.1	10364.4	10322	102.2	100.6
188	1163.4	1101.8	10436.3	10332	106.4	102.7
189						
Average:	1282.8	1179.7	10726.9	10440	100.33	94.4

12 IPM

	X Force (lbf)		Z Force (lbf)		Torque (lb-ft)	
Heat	Peak	Average	Peak	Average	Peak	Average
182						
183						
184	2077.2	2028.8	13684	13468	101.3	98.8
185						
186						
187	963.3	910.8	10312	10145	108	104.1
188						
189						
Average:	1520.3	1469.8	11998	11806	104.65	101.45

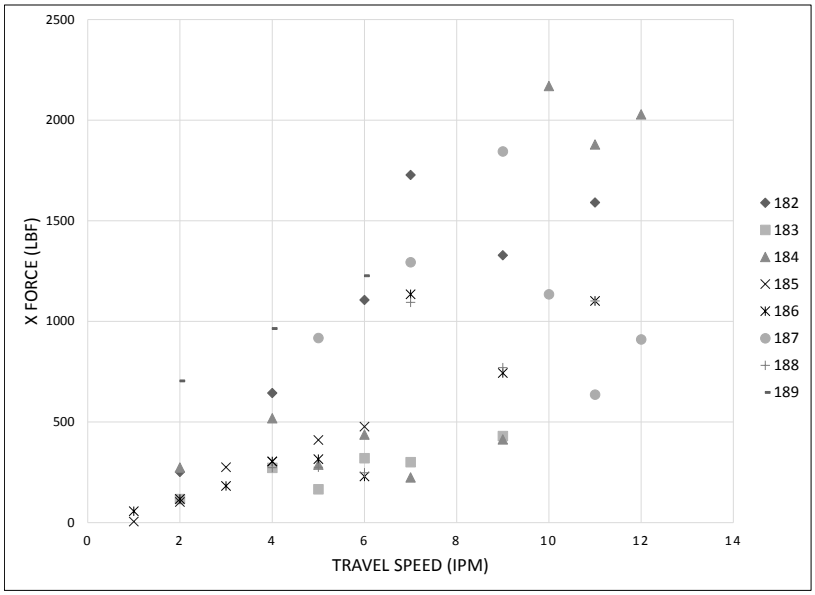

Figure E.1: The x force values experienced by each heat at each travel speed ran.

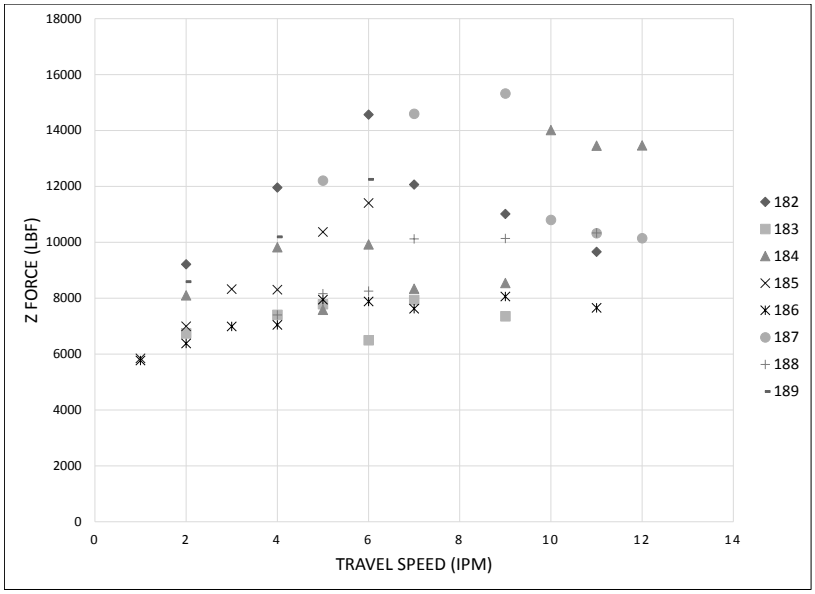

Figure E.2: The z force values experienced by each heat at each travel speed ran.

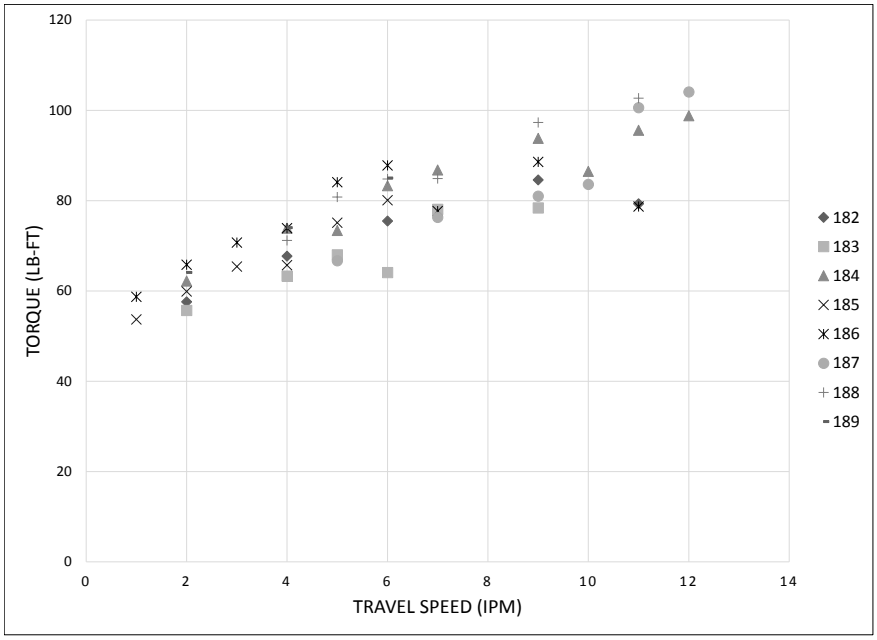

Figure E.3: The torque experienced by each heat at each travel speed ran.

APPENDIX F. WELD TEMPERATURES

Table F.1: Each weld consisted of three segments, each with a different travel speed. This table shows the welds run in the experimental heats, with their travel speed and measured tool temperature at each of the three segments. Because of changes in thermocouples between welds, the temperatures between welds can not be directly compared. The temperature data shows that temperature did not vary greatly within a weld, between its individual segments.

		Segment 1		Segment 2		Segment 3	
Heat	Weld #	Speed (ipm)	Temp (°C)	Speed (ipm)	Temp (°C)	Speed (ipm)	Temp (°C)
182	1	2	806	4	810	6	808
	2	7	860	9	855	11	840
183	1	2	798	4	800	6	794
	2	5	805	7	810	9	804
184	1	2	858	4	868	6	870
	2	5	851	7	850	9	846
	3	10	897	11	882	12	873.1
185	1	1	822	2	827	3	818
	2	4	819	5	812	6	811
186	1	1	856	2	875	3	872
	2	4	853	5	855	6	852
	3	7	808.5	9	825	11	832
187	1	5	804	7	805	9	800
	2	10	858	11	841	12	838
188	1	4	841	5	846	6	849
	2	7	882	9	884	11	886
189	1	2	885	4	881	6	873

APPENDIX G. WELD CONSOLIDATION AND PLATE SLIPPING

Table G.1: Each weld consisted of three segments, each with a different travel speed. This table shows the welds run in the experimental heats, with the weld quality at each travel speed. The occurrence of a plate slip during welding is also noted.

		Segment 1		Segment 2		Segment 3		
Heat	Weld #	Speed (ipm)	Fully Consolidated	Speed (ipm)	Fully Consolidated	Speed (ipm)	Fully Consolidated	Plate Slip
182	1	2	Yes	4	Yes	6	Yes	No
	2	7	No	9	No	11	No	Yes
183	1	2	Yes	4	Yes	6	No	No
	2	5	Yes	7	No	9	No	No
184	1	2	Yes	4	Yes	6	Yes	No
	2	5	Yes	7	Yes	9	Yes	No
	3	10	No	11	No	12	No	Yes
185	1	1	Yes	2	Yes	3	Yes	No
	2	4	Yes	5	Yes	6	Yes	No
186	1	1	Yes	2	Yes	3	Yes	No
	2	4	Yes	5	Yes	6	Yes	No
	3	7	No	9	No	11	No	Yes
187	1	2	Yes	4	Yes	6	Yes	No
	2	5	Yes	7	Yes	9	Yes	No
	3	10	No	11	No	12	No	Yes
188	1	4	Yes	5	Yes	6	Yes	No
	2	7	No	9	No	11	No	Yes
189	1	2	Yes	4	Yes	6	No	No